United Arab Emirates University

Scholarworks@UAEU

4-2023

INFLUENCING FACTORS OF IONIC-WIND IN A SPHERICAL STRUCTURE PROPULSION SYSTEM FOR SILENT AIRPLANE

Tha'er Khaled Ibrahem
United Arab Emirates University

Follow this and additional works at: https://scholarworks.uaeu.ac.ae/all_theses
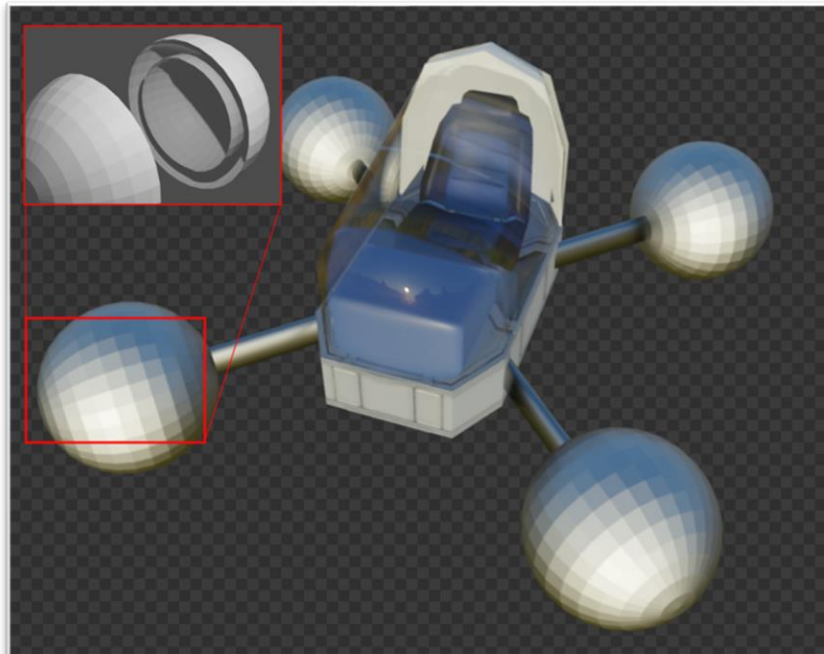
Part of the Electrical and Computer Engineering Commons

MASTER THESIS NO. 2023: 4

College of Engineering

Department of Electrical and Communication Engineering

INFLUENCING FACTORS OF IONIC-WIND IN A
SPHERICAL STRUCTURE PROPULSION SYSTEM FOR
SILENT AIRPLANE

Tha'er Khaled Shekh Ibrahem

April 2023

United Arab Emirates University

College of Engineering

Department of Electrical and Communication Engineering

INFLUENCING FACTORS OF IONIC-WIND IN A SPHERICAL STRUCTURE PROPULSION SYSTEM FOR SILENT AIRPLANE

Tha'er Khaled Shekh Ibrahem

This thesis is submitted in partial fulfillment of the requirements for the degree of Master of Science in Electrical Engineering

April 2023

Cover: Image related to a designed airplane to fly using spherical structure Ionic-Wind generators

(Photo: By Tha'er Khaled Shekh Ibrahem)

Declaration of Original Work

I, Tha'er Khaled Shekh Ibrahem, the undersigned, a graduate student at the United Arab Emirates University (UAEU), and the author of this thesis entitled "*Influencing Factors of Ionic-Wind in a Spherical Structure Propulsion System for Silent Airplane*", hereby, solemnly declare that this thesis is my own original research work that has been done and prepared by me under the supervision of Dr. Mahmoud F. Al Ahmad, in the College of Engineering at UAEU. This work has not previously formed the basis for the award of any academic degree, diploma, or a similar title at this or any other university. Any materials borrowed from other sources (whether published or unpublished) and relied upon or included in my thesis have been properly cited and acknowledged in accordance with appropriate academic conventions. I further declare that there is no potential conflict of interest with respect to the research, data collection, authorship, presentation and/or publication of this thesis.

Student's Signature:

Date: Apr 11, 2023

Approval of the Master Thesis

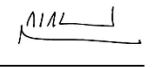This Master Thesis is approved by the following Examining Committee Members:

1) Advisor (Committee Chair): Prof. Mahmoud F. Al Ahmad
   Title: Professor
   Department of Electrical and Communication Engineering
   College of Engineering

   Signature _____ Date April 11, 2023

2) Member: Dr Saeed Al Nuaimi
   Title: Assistant Professor
   Department of Mechanical & Aerospace Engineering
   College of Engineering

   Signature _____ Date April 11, 2023

3) Member (External Examiner): Prof. Hugh Griffiths
   Title: Professor
   Department of Electronic & Electrical Engineering
   Institution: University College London, UK

   for Signature _____ Date April 11, 2023

This Master Thesis is accepted by:

Dean of the College of Engineering: Professor Mohamed H. Al-Marzouqi

Signature _Mohamed AlMarzouqi_

Date _April 28, 2023_

Dean of the College of Graduate Studies: Professor Ali Al-Marzouqi

Signature _Ali Hassan_

Date _May 2, 2023_

Abstract

Since the first airplane invented 100 years ago, most or all airplanes propulsion systems are based on moving parts powered by fossil-fuel which is impacting our environment by producing unwanted gases such as carbon dioxide, methane, greenhouse gases and more, furthermore, it is well known that there is a degradation in Oil & Gas resources on earth. Therefore, scientists are interested in finding an alternative way to fly an object. Recently, ionic wind-induced by Direct-Current (DC) Corona discharge have been introduced to enhance the future generation of airplanes without the need for moving objects. Corona discharge phenomena occurs when high potential differences of the order of tens of kilovolts between two asymmetrical electrodes do exists, which enable the generation of Electrohydrodynamic (EHD) thrust in the air. As of now, no "ion" airplane with such a solid-state propulsion system has yet flown. Hence, this study takes a close outlook to investigate such possibility. This work examines the use of a multi-directional thruster integrated in an airplane structure to enhance its flying performance. The proposed design is of spherical shape that incorporates several couple of layers to generate the required ionic wind distribution. The designed airplane is composed of a body that contains the pilot cabinet with all required control and sensory systems. The body is attached by four propellers (ionic wind generators) to provide the required thrust and direction. Each propeller consists of two spheres: outer sphere and inner one. The outer sphere is a sector of distributed multi-needle electrodes. The inner sphere is shaped like a net/mesh. The outer sphere is connected to positive polarity, while the inner is connected to the negative polarity of a voltage source. This arrangement will result in the generation of a strong electric field region to ionize the surrounding gases in the gap between both spheres. The generated ions will travel from the positive outer towards the negative inner mesh which will collide the neutral atoms on the way and generate the required wind, based on established design, which will be assembled with many ionic wind producers as a sectors of sphere, the power supply for each sector will be connected to a controller to control which sector to be on and which one to be off, it will be working as a switcher, then based on selected sectors, the direction of flight will be controlled accordingly.

Title and Abstract (in Arabic)

العوامل المؤثرة في الرياح الأيونية في نظام دفع الهيكل الكروي للطائرة الصامتة

منذ أول طائرة تم انتاجها واختراعها قبل نحو 100 سنة، معظم بل كل محركات الطائرات تعمل على مبدأ قطع متحركة بناء على مبدأ احتراق الوقود الأحفوري والتي تؤثر سلبا على البيئة من خلال انبعاث بعض الغازات الضارة مثلا ثاني أكسيد الكربون، الميثان، غازات الإحتباس الحراري وأكثر, علاوة على ذلك، إنه من المعلوم أن مصادر الطاقة في النفط والغاز في نقصان متواصل. لذلك أصبح الباحثون شغوفون بإيجاد طرق بديلة للطيران باستخدام طاقة كهربائية نظيفة. حاليا، هناك بعض الدراسات التي تبحث في إمكانية تحسين قياسات منتجات الهواء الأيوني التي تعتمد على فرق الجهد العالي ومبدأ (Corona Discharge) إلى درجات يمكنها منافسة الطائرات التقليدية. أساس الفكرة نشأت بناء على خاصية (Corona Discharge) والتي تنتج عند وجود فرق ضغط عالي بين قطبين بينهما وسط قابل للتأين مثل الغازات والهواء، فرق الضغط العالي يصل على عشرات الكيلو فولت، ولاستثمار هذه الخاصية في إنتاج الهواء الأيوني يتم توليد فرق الجهد بين قطبين مختلفين في الشكل، وهذا ما يسمى الكهروهيدروديناميكا. حتى الآن، لم يتم تصنيع طائرة تستطيع التحليق باستخدام الرياح الأيونية. من هنا، تهدف هذه الدراسة للتحقيق فيما إذا كان هذه الفكرة ممكنة عن طريق تصميم محركات تعتمد على الكهروهيدروديناميكا تستطيع التحليق في كل الاتجاهات، يتركز التصميم على بناء أربع محركات كروية الشكل على أطار المركبة وفي الوسط تحتوي المركبة على صندوق المعدات من مصدر الطاقة (بطاريات) ومتحكم وبعض المستشعرات والكاميرات, ويتكون كل محرك من كرتين داخل بعضهما البعض، الكرة الخارجية تتكون من مقاطع (لتحديد الاتجاهات) وكل مقطع يحتوي على إبر موزعة على السطح وموجهة للداخل بحيث تكون شحنة هذه الإبر موجبة لتقوم بتأين الغاز، وأما الكرة الداخلية فتم تصميمها على شكل شبكة وتكون موصولة على القطب السالب حتى تلتقط الأيونات المنتجة بين الكرتين، المجال الكهربائي العالي عند رؤوس الإبر يقوم بتأيين الغاز والذي بدوره ينتقل للقطب السالب الذي يحاط بمجال كهربائي خفيف، انتقال الأيونات بين السطحين يقوم بالتصادم مع ذرات الغاز المتعادلة وبالتالي ينتج هواء يسمى الهواء الايوني والذي يتكفل بإنتاج قوة دافعة في الاتجاه المعاكس. بناء على التصميم المقترح والذي يتكون من أربع محركات كروية وكل محرك يتكون من مقاطع أصغر من منتجات الهواء الأيوني، يمكن توصيل هذه المنتجات بالمتحكم الذي بدوره يعمل كمبدل أو صمام محدد لاختيار أي مقطع يجب تفعيله، بهذه الطريقة يمكن التحكم باتجاه الهواء المنتج وبالتالي التحكم باتجاه الطيران.

مفاهيم البحث الرئيسية: تفريغ إكليلي، مجال الكهرباء الساكنة، مسافة الفجوة، الرياح الأيونية، الدفع، طائرة صامته أقطاب متعددة الإبر والأقطاب الشبكية.

Author Profile

Tha'er Shekh Ibrahem holds bachelor's degree in electrical engineering from An Najah National University – Palestine, since 2017. Currently, He works as a Customer Service Manager at INNIO Waukesha Gas Engines, Abu Dhabi/UAE. In addition to that, he is studying Master of Science in electrical engineering at United Arab Emirates University. He has received the "2022 UAE Engineering Challenge" organized by Elsevier. His current research interests focus on the design and implementation of ion-based airplanes.

Acknowledgements

All thanks and praise to Almighty Allah for all the graces He granted to me along with my life.

I would like to thank my committee for their guidance, support, and assistance throughout my preparation of this thesis. My immense appreciation to Dr. Mahmoud F. Al Ahmad for his kindness, mentorship, and generosity for the support he gave me to fulfill my aspiration.

Furthermore, special thanks go to my parents, family, and friends for their unconditional support and encouragement.

Dedication

To my beloved parents who gave their lives to be who I am, and to my soulmate my wife

for her extraordinary support and encouragement.

Table of Contents

List of Tables

List of Figures

List of Abbreviations

EAD	Electroaerodynamics
EHD	Electrohydrodynamics
NS	Navier-Stokes
NTP	Non-Thermal Plasma

Chapter 1: Introduction

1.1 Overview

Since the first manufactured airplane has been invented 100 years ago, most airplanes are powered by moving parts propulsion systems using fossil-fuel combustion (Xu et al., 2018). Due to the lack of fossil fuel on earth and the catastrophic impact of carbon dioxide emissions affecting the environment and ozone layer, in recent decades, researchers' interest focused on finding an alternative method to fly an object using a clean electric propulsion system such as Electroaerodynamics (EAD) principle where electric field accelerates ions in fluid (Air). In this field, the EAD is built based on corona discharge phenomena generated using a high voltage difference between two asymmetrical electrodes, one sharply pointed electrode, and a larger radius ground electrode, accordingly, the electric field will ionize the fluid between both electrodes and force the ions to move toward a certain direction generating an ionic wind and thrust. Up to date, researchers are studying several aspects such as structure design, electrodes arrangements, and applied voltages to enhance the resultant ionic wind speed and thrust force trying to find an answer to whether this thrust could be scaled to figures that compete with the conventional airplanes propulsion systems (H. D. Perkins & Thompson, 2009).

This research aims to identify two main points; firstly, the best achievable ionic wind speed and thrust density using the optimum electrode structure that can be used in future airplanes. This chapter will introduce the study by first discussing the background and context, followed by the research problem, the research objectives, the significance, and finally, the limitations.

1.2 Statement of the Problem

Corona discharge phenomena can be observed when a spark appears between a couple of electrodes having a high voltage potential, one highly curved electrode called " Emitter " and another less curved electrode " Collector ", it's created with a high voltage and low current system, corona discharge starts when the high electric field between both electrodes exceeds the breakdown voltage of the medium, during corona discharge

a high electric field strength around emitter ionize the air – or another medium –, electric field force the ions to move towards the collector and collide the other neutral atoms during along the way, which is called ionic wind (H. D. Perkins & Thompson, 2009) (Figure 1).
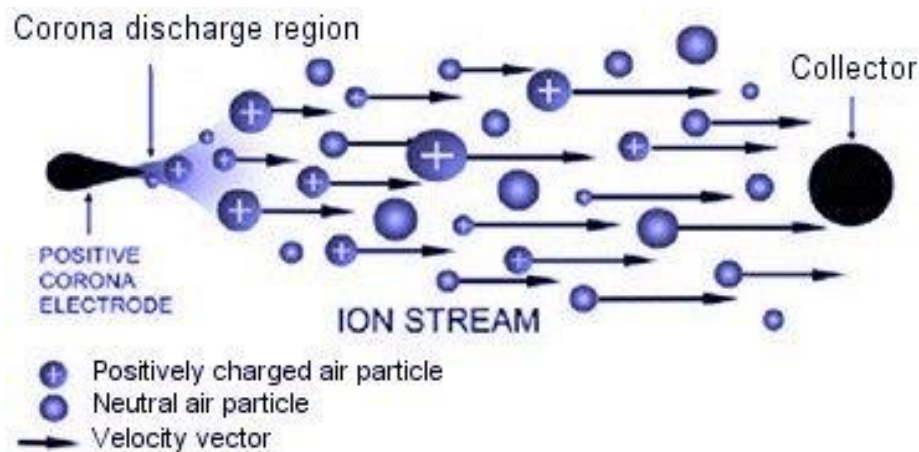
Figure 1: Ionic Wind Illustration

The ionic wind phenomena were initially discovered by Hauksbee in 1709. Then experimentally Chattock found the relationship between the ionic wind and the characteristics of voltage and current in 1899. In 1986, Sigmond proposed a theoretical design of a needle-to-plate system to generate a corona discharge (Lv et al., 2019a), since then, those studies allocated the basics of subsequent research to utilize ionic wind in many applications such as thermal cooling, flow control and ionizing blowers (T. Zhang et al., 2019).

As mentioned earlier, several studies were conducted between 2008 and 2018 by changing the configuration of electrodes structure and measuring the resultant ionic wind velocity, comparing all these studies revealed that the velocity and efficiency of the ionic wind generated by Needle-to-Net electrode are higher than Needle-to-Ring structure (Lv et al., 2019a). In 2018, Dr. Barrett and his team designed and successfully flew an unmanned airplane for 40 – 45 m and a speed of 4.8 m/s using the same concept built with a 5 m wingspan attached to two stages of the wire-to-cylinder propulsion system (Xu et al., 2018) (Figure 2).
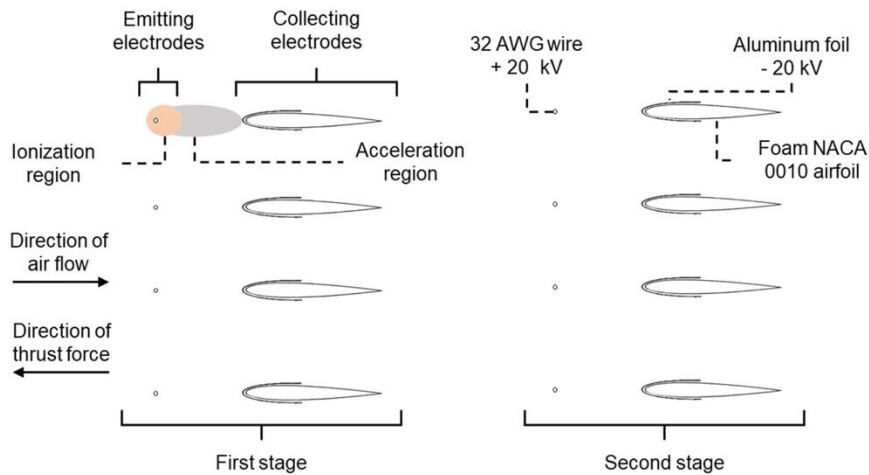
Figure 2: Two Stages of Wire to Cylinder Structure.

As a result, existing researches are inconsistent in terms of the best electrode structure and resultant ionic wind velocity, furthermore, the model developed by (Xu et al., 2018) didn't take into consideration the direction of flying and the ability to control speed and direction. Therefore, what if we enhance the Multi-Needle to Net-Electrode's structure in a shape that is applicable to be attached with a multi-directional and controllable flying object?

1.3 Research Aims, Objectives, and Questions

Given the inconsistency of the existing studies regarding the maximum ionic wind velocity and lack of optimum propulsion system design that can be utilized for a controllable flying object, this study will aim to figure out a new propulsion system that competes for the available structures in terms of ionic wind velocity and ability to be controlled.

To achieve the aim of this research, the specific objective will be outlined and described as the following:

Objective #1: To compare the available studies of ionic wind generators in terms of the resultant ionic wind velocity.

Objective #2: To calculate the ionic wind velocity of new designed spherical structure experimentally and explain its advantages in terms of stability and control.

Consistently with the research objectives, the following questions outline the research expected results.

RQ #1: What was the maximum ionic wind velocity achieved by previous studies? And what was the structure used to achieve that maximum velocity?

RQ #2: What is the ionic wind velocity resulting from new designed spherical structure?

1.4 Relevant Significance

Humans burn fossil fuel more and more to power cars, airplanes and other machines, these waste gases including carbon dioxide are catastrophically impacting the world climate change and extensively contributing to global warming and the greenhouse effect, therefore the leaders in the world including scientists and researchers are racing to give away of fossil-fuel source and investing more in green energy vehicles and machines.

And hence, this study will contribute to the race of getting closer to clean and silent airplanes around the world, furthermore, the utilization of EAD of drones will give a new technology to manufacture unmanned airplanes which record videos without background noise since the new airplanes are silent, to more specific and practical, this study will link between the technical studies that address the best values of the system and the ability to be commercially viable.

Nevertheless, taking into consideration the EAD limitations to be used as an engine of an airplane, the ionic wind velocity increases as the higher voltage is applied, but a high voltage will generate a spark at a certain level. Therefore, there will be a limited range of power and thus EAD doesn't seem could be used to power a large airplane (H. D. Perkins & Thompson, 2009). Even though, the studies afterward including this research aim to fill this gap. On the other hand, there will be a lack of resources to build a complete system to be verified and tested.

1.5 Research Organization

The thesis is organized as follows:

Chapter 1 (Introduction): In this chapter, the basic concept of corona discharge and ionic wind generation will be studied from the scratches.

Chapter 2 (Literature Review): It gives a background about the corona discharge and ionic wind concept; it also goes through the previous research related to ionic wind characteristics and the structures that have been studied.

Chapter 3 (Methodology and Simulation): This chapter introduces the new structure design and discusses the possible ways to verify and validate the resultant ionic wind velocity, additionally it represents the results of the simulation for this design.

Chapter 4 (Conclusion): Chapter four concludes the thesis results, clarifies the limitations and challenges faced during the study, and proposes future work.

Chapter 2: Literature Review

This chapter gives a background about the corona discharge and ionic wind concept; it also goes through the previous research related to ionic wind characteristics and the structures that have been studied.

After the first observation of the ionic wind phenomena by F. Hauksbee in the 1700s, this phenomenon became a popular scientific subject and numerous scientists such as M. Faraday and J. C. Maxwell (Park et al., 2018) paid attention to characterize and analyze the parameters of the corona discharge and ionic wind. In recent decades, experiment-based studies with improved instruments enabled researchers to explore unexpected aspects and pieces of evidence of the phenomena trying to figure out whether it can be advanced to achieve higher ionic wind scales that can be an alternative method to the conventional ones such as heat dissipation devices which rely on fans, this is because of the advantages of ionic wind concept such as low power consumption, high power efficiency, free of moving parts and smaller instruments.

2.1 Theory of Corona Discharge

The name of corona comes from the Latin word "Crown", the name started from the day of phenomena observation which started by the sailors during stormy weather at sea, they noticed a bluish light on the top of worn masts, so it was seen as a crown or halo around the head of mast (J. Perkins, 2009). Several years later, phenomena were observed during high-voltage experiments conducted in the laboratory; therefore, it was referred to as a corona reference to the previous papers written by Latin-oriented scholars.

Generally, ASTM standards defined corona as a visible discharge that breaks the insulation between conductors, it is created by a gaseous ionization between two asymmetrical conductors having voltage difference, starts when the electric field exceeds a critical value when some electrons of neutral atoms became free. The impressive glow of the corona is the visualization of photons released in the recombination of electrons and positive ions to form a neutral atom again. Corona discharge consumes low energy

refers to the scale of the voltage and current, it is required a few KV to be generated but the current is very low and usually 10^{-10} to 10^{-4} A.

However, the corona discharge process has existed for over 100 years, since then, the corona has been widely utilized in several applications commercially such as electrostatic precipitation, electrophotography, static control in semiconductors manufacturing, ionization instruments, and control of acid gases from combustion destruction (Chang et al., 1991). Furthermore, remarkable applications we've seen during literature reviews such as "Ioncrafts" which will be discussed in detail in this thesis as it's the main application of corona discharge and ionic wind, Ioncrafts also known as Electrohydrodynamic lifter "EHD Lifter"; it is kind of lightweight vehicles to lift off and hover when ionic wind velocity and thrust force exceed the weight of the vehicle, there are other applications of corona discharge phenomena such as EHD cooling systems, plasma actuators, and electrical generators.

Generally, the applications of EHD wind or in other words ionic wind serve human and offers the ability to control the wind through electrostatic force to chive lift, modify boundary layers, heat dissipation, etc.

The characteristics of corona discharge were studied by (J. S. Townsend, 1915) when he figured out an approximate relation between voltage and current of a stable corona discharge, generally, the relationship is given by the following equation.

$$i = k\Phi(\Phi - \Phi_0) \tag{2.1}$$

Where i is current, Φ is the applied voltage, Φ_0 is the onset voltage which is the minimum voltage required to ignite a steady-state corona discharge, and k is a constant depending on the configuration of the system such as the radius of the sharp edge, the shape of the collector, and the gap distance between both electrodes, it depends also on the properties of the gas such as ion mobility and permittivity.

In addition to the above, (Peek, 1920) derived the minimum gap distance required to start a stable corona discharge experimentally, he used the electric field distribution in a simple geometry, besides that, he figured out the minimum voltage required to start the

corona (onset voltage). For example, for a wire-to-plate configuration, he found that the minimum gap distance (d) required to ignite a corona is $2.925 \times r_0$, where r_0 is the radius of the wire. Moreover, Peek's law defines the minimum electric field on the wire required to start a stable corona discharge, which is given in the following relation.

$$E_0 = E_c m_v \delta^2 \left(1 + \frac{0.0301}{\sqrt{\delta.r_0}}\right) \tag{2.2}$$

Where E_0 is the magnitude of the electric field on the wire at onset voltage, E_c is the disruptive critical voltage gradient, it's about 3×106 V/m for air, m_v is the factor of the wire surface contamination, and δ is the gas density factor which is based on the pressure (P) in cm of Hg and temperature (T) in degrees Celsius and given as per the following relation.

$$\delta = \frac{3.92\,P}{273+T} \tag{2.3}$$

The electric field on the wire (E_w) can be written in terms of applied voltage (Φ)

$$E_w = \frac{\Phi}{r_0 \ln\left(\frac{2d}{r_0}\right)} \tag{2.4}$$

And by substituting equation (2.4) into (2.2) the onset voltage can be given as per the following formula.

$$\Phi_0 = E_c m_v \delta^2 r_0 \left(1 + \frac{0.0301}{\sqrt{\delta.r_0}}\right).\ln\left(\frac{2d}{r_0}\right) \tag{2.5}$$

2.2 Generation of the Ionic Wind

Initially, to simplify the concept of ionic wind generation using corona discharge phenomena, a positive corona discharge between needle and plate is shown in Figure 3. To ionize the air molecules (or another medium) the electric field magnitude should exceed a certain critical value depending on medium characteristics, unlike a discharge between two parallel plates where the electric field is uniform, in corona discharge, the field strength is high near the sharp electrode led to ionize the air around the sharp edge and called Ionization Zone.
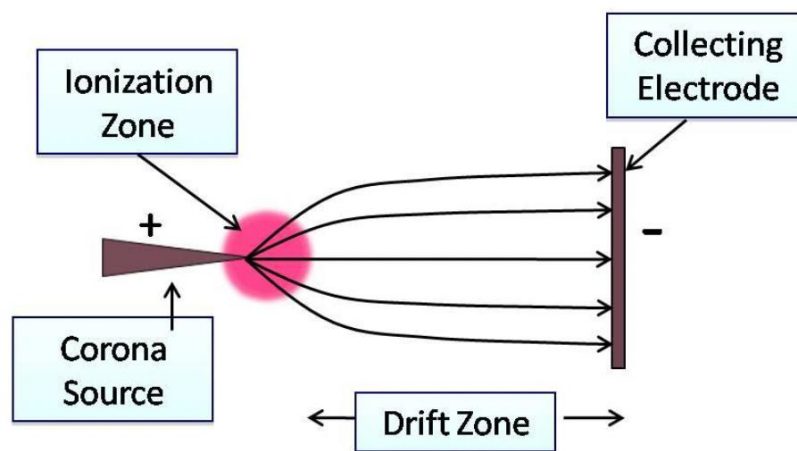
Figure 3: Positive Corona Discharge Schematic

Ionization will be localized in Ionization Zone and corona discharge is thus said to be a locally ionized plasma. Farther away from the needle (Sharp Edge), the electric field magnitude becomes lower than the critical value and then there will be no ionization. Importantly, based on the above, there will be a limited voltage potential between both electrodes to generate an ionic wind depending on the structure of the system and gas characteristics, to maintain the system at this state voltage potential should be high enough to create an ionization zone without exceeding a certain value where the electric field would ionize the whole gas along the gap and accordingly create a spark. The ions are created in the ionization zone under the influence of the electric field and then drift through the region beyond the ionization zone towards the collecting electrode, therefore the area beyond the ionization zone is called Drift Zone, during the

travel of ions toward the collecting electrode, ions collide with neutral molecules and transfer their momentum as shown in Figure 4, finally, the ionic wind is generated toward a certain direction.
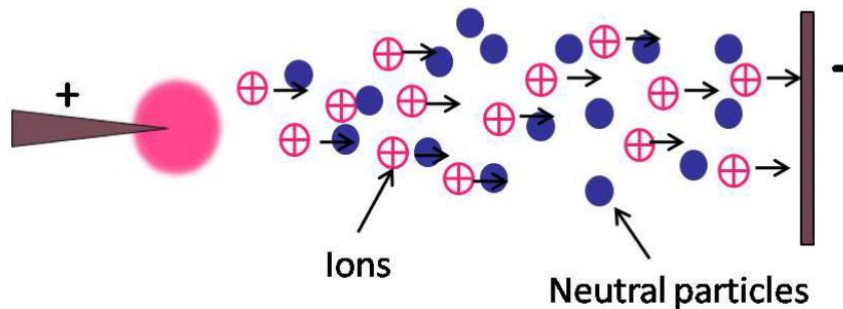
Figure 4: Ionic Wind Flow.

Studies of ionic wind concept and ionic wind blowers are split into two main areas, some simulate the ionization zone and others studied the drift region, former researchers were interested in studying the ionization zone and the chemical reactions within that ionization region, then when researchers became interested in applications of ionic wind, detailed studies shed some light on drift region to study the characteristics of EHD flow. The following subsections review some of these substantial works.

2.2.1 Ionization Zone

Numerous works studied the ionization zone and its chemical reactions, a remarkable study was done by (Chen & Davidson, 2003) who modeled the ionization zone and its domain as shown in Figure 5, where the gray-colored region indicates the zone, the boundary of the ionization zone is the distance at which the electrical field magnitude becomes lower than the critical value.

Figure 5: Simulated Ionization Zone

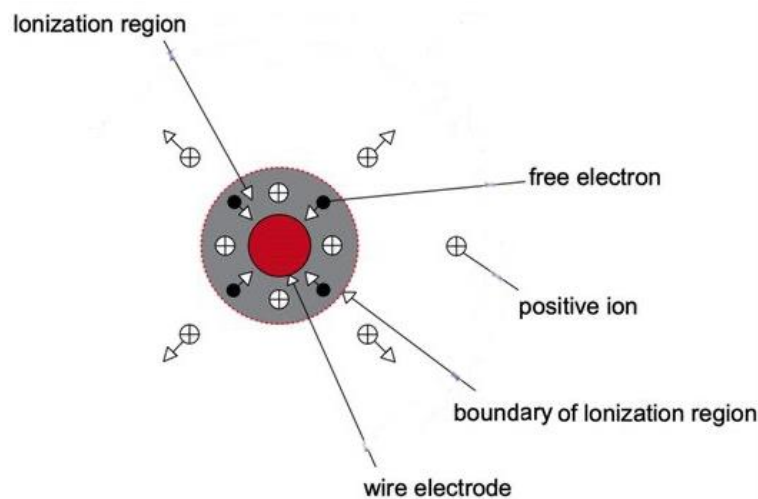Their study considered the charged particles as collective, positive ions, negative ions, and electrons; accordingly, the governing equations were the drift equations for the ions and the drift-diffusion equation for the electrons, those equations will be explained in detail in Section 2.3.

2.2.2 Drift Zone

Most researchers interested in applications of corona discharges dismiss the study of ionization since the zone is small compared to the drift zone, many studies in literature modeled the ion transport in the drift zone (Adamiak & Atten, 2004; Go et al., 2007; Tirumala & Go, 2011). All these studies followed the same procedure for the simulation of corona discharge, the difference was in the numerical techniques used to model the equations.

They mainly used Poisson's equation and ion transport equation coupled together to simulate the model, in these models, the ionization zone is neglected, and they focus on drift region, therefore, only positive ions were considered in the DC positive corona discharge, a detailed explanation of the governing equations for the drift zone will be discussed in Section 2.3.

Consistent with this thesis, very few studies simulated the corona discharge in multiple electrode systems, (Deng & Adamiak, 1999) simulated a tri-electrode system where the corona discharge was generated between needle and grid with a plate behind the grid, but their numerical results were not validated experimentally, therefore, it's difficult to argue the procedure.

2.3 Theoretical Background and Model

To develop a design methodology for an ionic wind generator, it is mandatory to completely understand the basic theory and model of corona discharge and ionic wind generators in terms of the basic model used to derive the governing equations and main parameters that all reviewed designs followed, in this section, theoretical background and model will be thoroughly explained to elucidate the governing equations required for numerical calculations of ionic wind velocity and other parameters of the design such as onset electric field intensity.

A remarkable semi-empirical theory was proposed by (Warburg, 1899), Warburg's law explains the distribution of current density on the collector electrode in a system of point to a plate, but this theory can be applied to other geometries where the collector is a plate, the law is given as the following equation.

$$j(x) = j(0)\cos(\theta)^m \; ; \; \theta = \tan^{-1}\left(\frac{x}{d}\right). \tag{2.6}$$

Where j (x) is the current density on the plate x from the center, j (0) is the current density at the center, and d is the gap distance between the needle (emitter electrode) and the plate, Figure 6 shows the geometric arrangement that Warburg concluded this theory.
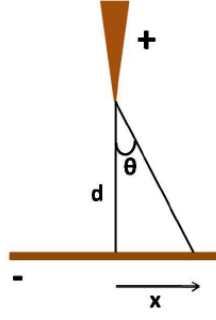
Figure 6: Geometric Illustration of Warburg's Theory.

Interestingly, the most known study of corona discharge ionic wind was performed by (Stuetzer, 1959), who mainly assumed the momentum transfer collisions of ions with neutral air atoms as a body force in the Navier-Stokes (NS) equations as shown in equation 2.7.

$$q \left(\frac{\partial \vec{u}}{\partial t} + \vec{u} . \nabla \vec{u} \right) = -\nabla p + v \nabla^2 \vec{u} + \left(q_{sc} \vec{E} \right) \tag{2.7}$$

The body force term is given by the last term $q_{sc}\vec{E}$, where q_{sc} is the space charge density, and $\vec{E}$ is the electric field.

Furthermore, the pressure drop across the gap in a wire-to-plate configuration is given by equation 2.8 which is derived based on the Navier-Stokes equation in static equilibrium where there is no flow condition and after comparing the terms of the equation.

$$\Delta p \approx \frac{i}{b} \frac{d}{A} \ln \left(\frac{2d}{r_0} \right) \tag{2.8}$$

Where Δp is the pressure drop, i is current, A is the area of the collector electrode, b is the ion mobility in air, d is the gap distance, and r_0 is the wire radius as mentioned before. After substituting Townsend's equation (Equation 2.1) into Equation 2.8 the pressure can be given in terms of applied potential, accordingly, the consumed power in corona discharge is given as:

$$P = \Phi i = k\Phi^2(\Phi - \Phi_0) \tag{2.9}$$

In addition to the above, Stuetzer defined the efficiency of corona discharge to be calculated by comparing the output kinetic energy with electrical energy which is given as shown in relation (2.10).

$$\eta = \frac{dynamic\ pressure\ power}{total\ power\ consumed} = \frac{\Delta p}{P} = \frac{(dm/dt)u^2}{\Phi i} = \frac{\rho Q^3}{kA^2\Phi^2(\Phi - \Phi_0)} \tag{2.10}$$

Where ρ is the density of the gas, u is the velocity, Q is the volume flow rate, and A is the flow area that can be found based on configuration.

The model of corona discharge is mainly relying on solving Poisson's equation (Equation 2.11) which is a generalization of Laplace's equation, in other words, the potential V is governed by this equation(Rickard & Dunn-Rankin, 2007).

$$\nabla^2 V = \frac{-q}{\varepsilon_0} \tag{2.11}$$

Where q is the space charge density, and ε_0 is the dielectric permittivity of air $(8.8542 \times 10^{12}\ F/m)$.

Then the electric potential can be given by electric field intensity as the following equation.

$$E = -\nabla V. \tag{2.12}$$

Concerning the Section 2.2 literature review, the transport equation to be solved for each particle, electrons, positive ions, and negative ions can be represented as:

$$J = \mu_E q\vec{E} + q\vec{u} - D\nabla q \tag{2.13}$$

Where J is the current density generated by diffusion, conduction, and convection, μ_E is the ion's mobility in the air ($2.7 \times 10^{-4}\ {m^2}/{V.s}$), D is the diffusion coefficient ($5.5 \times 10^{-6}\ {m^2}/{s}$).

The transport equation 2.13 can be simplified by considering the charged particles' velocity is far larger than the airflow velocity and diffusivity coefficient of ions, subsequently, the transport equation is defined as:

$$J = \mu_E q \vec{E} \qquad\qquad (2.14)$$

Conversely, the current density should satisfy the continuity equation which is about the conservation of charge (Equation 2.15).

$$\nabla J = 0 \qquad\qquad (2.15)$$

Finally, for incompressible Newtonian fluid, the ionic wind velocity can be calculated by the continuity equation (Equation 2.15) and the Navier-Stokes equation (Equation 2.7).

2.4 Effect of Electrodes Structure

In recent history, corona discharge and ionic wind have been a field of study since the early 20th century, as mentioned earlier, ionic wind and corona discharge have become of paramount importance in several applications, and researchers interested in the investigation of ionic wind enhancement throughout studying the resultant ionic wind velocity and system efficiency of numerous designs. Particularly, the structure of the propulsion system plays a key factor in ionic wind velocity, in this section, works of literature are reviewed in terms of the electrode structure.

2.4.1 Wire-to-Cylinder Structure.

There are numerous types of research studied structures in different approaches during the past couple of decades is the Wire-to-Cylinder structure, (Fylladitakis & Kiousis, 2008; Gilmore & Barrett, 2015; Lee et al., 2022; Xu et al., 2018). Fylladitakis and Kiousis verified the relationship between the current, applied voltage, and ionic wind velocity experimentally and theoretically, as shown in Figure 7 (Fylladitakis & Kiousis, 2008). 300 mm long electrodes were used where the emitter wire and collector cylinder were made of copper and aluminum respectively.
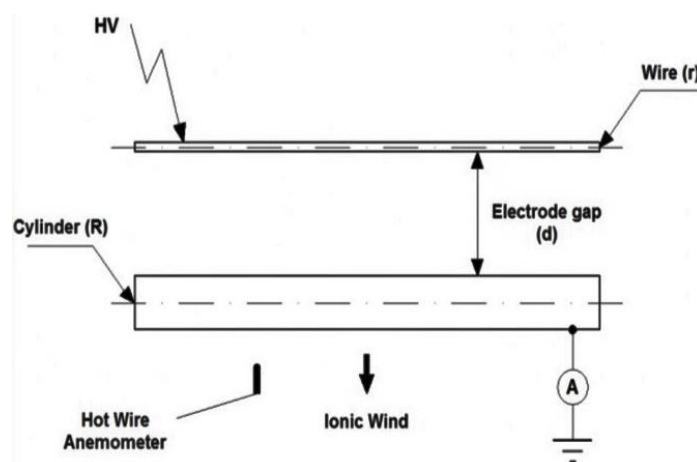

Figure 7: Schematic View of the Experimental Setup.

Consistent with the numerical model, in this structure, the ionic wind velocity is approximately linear with applied voltage but proportional to the square root of the discharge current, and the velocity decreases as the gap distance between the wire and cylinder increases, furthermore, the wind velocity has an inversely proportional relationship with the wire radius, while the cylinder radius has a small effect on ionic wind velocity because of its effect on electric field intensity in the emitter's surface due to the higher field inhomogeneity. Nevertheless, the maximum ionic wind velocity was empirically found 2.88 m/s at 20 kV applied voltage, the efficiency of the Wire-to-Cylinder system is low (0.8 %) and the system doesn't seem quite efficient.

Steven Barrett, associate professor of aeronautics and astronautics at MIT (Massachusetts Institute of Technology) was inspired by the shuttles that glided through the air silently without any moving parts, accordingly, he studied the ionic wind concept

in terms of thrust-to-power ratio and thrust density to compare the results with conventional airplanes and figure out whether it's a viable solution to use the ionic wind as an unmanned airplane (Jennifer Chu, n.d.). Interestingly, Barret conducted a theoretical analysis and experimentally found that the EHD propulsion system can provide a practical level of efficiency compared to conventional flights whilst the thrust density is still under investigation (Gilmore & Barrett, 2015; Masuyama & Barrett, 2013).

Multistage electrodes were used to improve the ionic wind speed and accordingly the thrust values as shown in Figure 8 (Gilmore & Barrett, 2015) as an illustration of an empirical study conducted in 2015 when it was again reconfirmed that the thrust-to-power ratios of the EHD system are comparable with that of conventional propulsions.
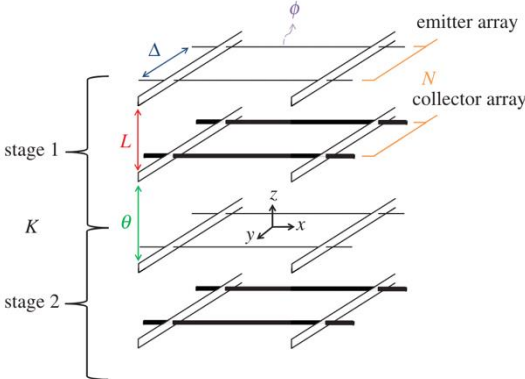

Figure 8: Illustration of Electrodes Arrays.

L is the electrode gap distance, Δ is the electrode spacing between pairs, θ is the distance between electrode pair stages, ϕ is the emitter electrode wire diameter, N is the number of electrode pairs per stage and K is the number of stages.

For this propulsion system design, the author derived the expression of the thrust (Equation 2.16) and thrust-to-power ratio expression (Equation 2.17) where "I" is the current generated by the system, "L" is the distance between the emitter and collector, "µ" is the ion mobility and "V" is the applied voltage.

$$T = \frac{IL}{\mu} \qquad (2.16)$$

$$\frac{T}{P} = \frac{L}{\mu V} \qquad (2.17)$$

Experimentally, the emitter electrodes were made of 0.202 mm or 0.0799 mm diameter tinned copper wires, and the collectors were 6.35 mm diameter Aluminum tubes where the inception voltage was 70 kV according to Peek's law corresponding to the air gap used in their study (30 and 50 mm).

About the structure that Barrett used to study the ionic wind generator as a propulsion system, the maximum thrust-to-power ratio found is 110 N/KW while it's only 2 N/KW for the jet engine, but the main couple of parameters studied to compare whether the EHD propulsion system would compete the conventional systems such as turbines or jet engines were inversely proportional, as per Table 1, an increase of thrust per unit area (Thrust Density) would decrease the thrust-to-power ratio.

Table 1: Comparison of Thrust-to-Power ratios with Thrust Density.

Thrust Density (N/m^2)	1	1.5	2	2.5
L = 30 mm	7.9	7.0	6.3	5.8
L = 50 mm	10.2	8.9	7.9	6.8

However, the study unveiled that the thrust-to-power ratio decreases with increasing power and thrust, on the other hand, increasing thrust density would decrease the thrust-to-power ratio, where thrust density can be increased by increasing the power supply or by decreasing the working area, furthermore, long air gap distance generates higher thrust-to-power ratio for a given thrust per unit area.

In addition to the above, Mr. Barrett and his team at MIT unveiled an impressive result later in 2018 (Xu et al., 2018), they were successfully able to demonstrate the first-ever silent airplane operating with a solid-state propulsion system using the ionic wind

concept. As illustrated in Figure 2 in the introduction chapter, the propulsion system was made based on a Wire-to-Cylinder structure, two stages of electrodes and each stage consist of four couples of emitter and collector, the emitter electrodes were made of 32 American Wire Gauge (32 AWG; 0.2 mm diameter) stainless steel wire, gap distance was fixed at 60 mm between emitter and collector, and the collector electrodes were a National Advisory Committee for Aeronautics (NACA) 0010 airfoiled foam section and covered in a thin layer of aluminum foil.

However, the study unveiled that the thrust-to-power ratio decreases with increasing power and thrust, on the other hand, increasing thrust density would decrease the thrust-to-power ratio, where thrust density can be increased by increasing the power supply or by decreasing the working area, furthermore, long air gap distance generates higher thrust-to-power ratio for a given thrust per unit area.

In addition to the above, Mr. Barrett and his team at MIT unveiled an impressive result later in 2018 (Xu et al., 2018), they were successfully able to demonstrate the first-ever silent airplane shown in Figure 9 operating with a solid-state propulsion system using the ionic wind concept. As illustrated in Figure 2 in the introduction chapter, the propulsion system was made based on a Wire-to-Cylinder structure, two stages of electrodes and each stage consist of four couples of emitter and collector, the emitter electrodes were made of 32 American Wire Gauge (32 AWG; 0.2 mm diameter) stainless steel wire, gap distance was fixed at 60 mm between emitter and collector, and the collector electrodes were a National Advisory Committee for Aeronautics (NACA) 0010 airfoiled foam section and covered in a thin layer of aluminum foil.
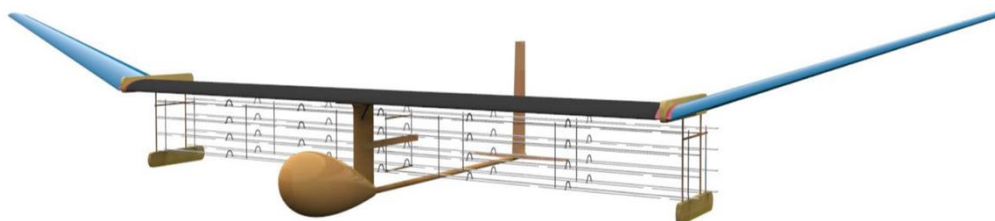

Figure 9: EAD Silent Aeroplan Design.

The power supply system was built of 54 X 3.7 V Lithium-Ion batteries connected in series giving a 200 V output, accordingly a High-Voltage Power Converter (HVPC) was used to gain the voltage by around 210 X and feed the propulsion system with around 42 kV required to create a corona discharge and ionic wind.

This demonstration is an innovative work from Mr. Barrett and his team and is ambitious to answer the question of whether the ionic wind could be an alternative power propulsion system for future airplanes, nevertheless, the author finds the door open to finding an improved design to make the airplane able to be controlled in a multi-directions and outdoor environment.

2.4.2 Needle-to-Ring Structure.

The Needle-to-Ring structure has been studied in terms of I-V characteristics and resultant ionic wind velocity profile, the wind velocity in this structure is higher than Wire-to-Cylinder which was proven experimentally and supported by a theoretical explanation by (T. Zhang et al., 2019; Y. Zhang et al., 2015).

This structure was designed considering the emitter electrode is a needle with 100 μm radius curvature and the collector electrode is a copper ring with an inner radius of 1 cm and external radius is 2 cm, both electrodes were fixed opposite to each other with a variable gap distance from 1 to 3 cm and the supplied voltage was from 0 to 25 kV on the needle side for positive corona discharge.

As expected for all structures, the corona inception is proportional to the gap distance, in addition to that, a larger gap distance decreases the ionic wind velocity, on the other side the ionic wind increases linearly at the center of the ring concerning the applied voltage as shown in Figure 10 (Y. Zhang et al., 2015).
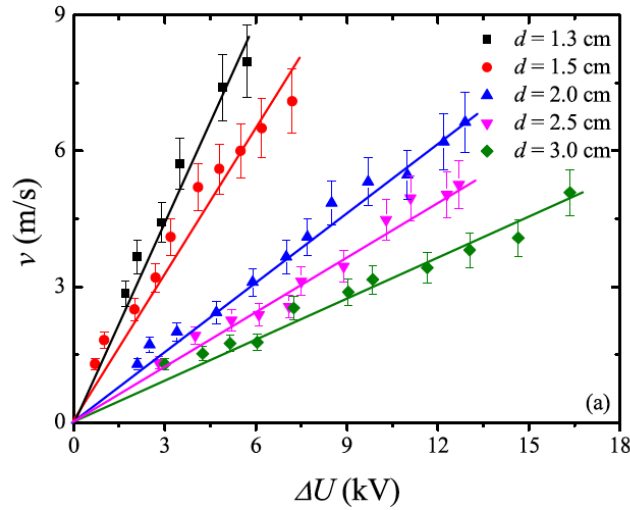
Figure 10: Wind Velocity at Different Gap Distance.

During these reviewed studies, both corona discharges (Positive and Negative) were investigated and compared in addition to the other aspects of research aims, the ionic wind velocity was always higher in the positive corona compared with the negative corona. Additionally, the ionic wind velocity profile showed that the wind distribution is more homogeneous in negative corona which is caused by the different discharge mechanisms as shown in Figure 11 (T. Zhang et al., 2019).
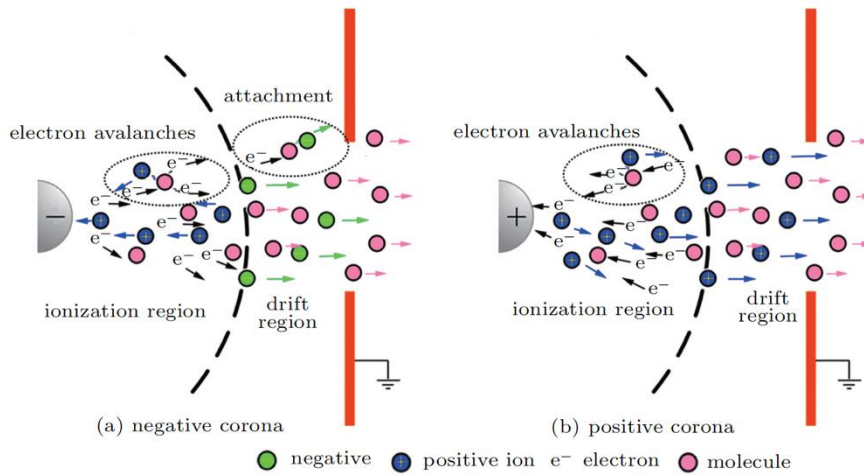

Figure 11: Discharge Mechanism in Positive & Negative Corona.

Generally, it is obvious that the ionic wind velocity in the Needle-to-Ring structure is higher than Wire-to-Cylinder structure, within the literature, the ionic wind velocity of the Wire-to-Cylinder was almost 3 m/s while as shown in Figure 10, the

maximum velocity of the ionic wind was achieved to around 8 m/s at 6 kV in the structure of Needle-to-Ring, this is related to the concept of discharge mechanism of air molecules and electric field profile within different structures, based on that, it is possible to figure out an optimum design for a propulsion system that can be used as an engine of the silent airplane.

2.4.3 Multi-Needle-to-Net Structure.

Recently, some researchers tried to study the concept of ionic wind from the aspect of the resultant wind velocity by designing a multi-needle emitter electrode and a net structured collector electrode (Lv et al., 2019; G. W. Zhang et al., 2021). The emitter electrode consists of some needles with a certain diameter and tip curvature, on the other side, the mesh or net electrode was studied with different mesh side lengths to figure out the resultant wind speed, to simplify the structure, Figure 12 shows the illustration of the structure.
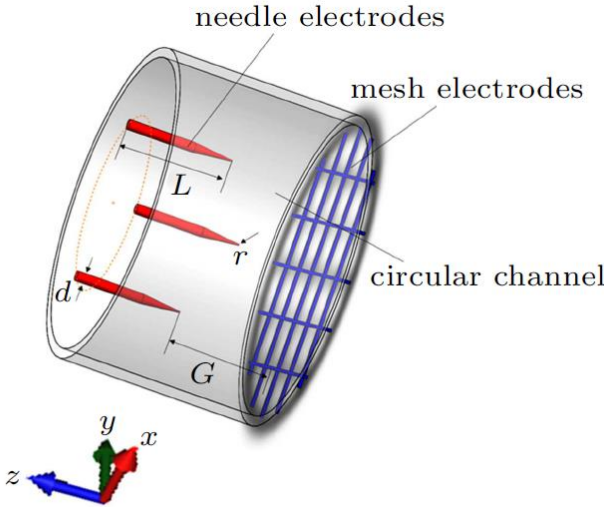

Figure 12: Multi-Needle to Net Structure.

Lv et al. (2019) has done an interesting study on this structure empirically and numerically, and the results showed that 8 m/s wind velocity could be achieved at a certain condition of the structure, the velocity varies based on other variables in the structure such as the needle distribution, gap distance, and mesh side length. Accordingly, the factors affecting the velocity of the wind are listed as the following:

1. The number and distribution of needle electrodes.
2. The side length of meshes of the net-electrode.
3. Voltage amplitude is applied to the needle electrodes.
4. The gap distance between both electrodes.

Based on the above, the researcher used five different distributions where 33 needles were used in a uniform distribution which resulted in the maximum wind velocity. Technically, the reason behind this factor is that the electric field distribution for a particular needle in the structure is affecting another needle's electric field. On the other hand, three different side lengths were utilized (2, 0.85, and 0.425) mm, and experimentally, the maximum ionic wind velocity resulted from a 0.85 mm side length structure, therefore, it is obvious that there will be an optimum design that can be manufactured to provide the maximum wind velocity, and to clarify above design variables, Figure 13 shows both electrodes arrangement.
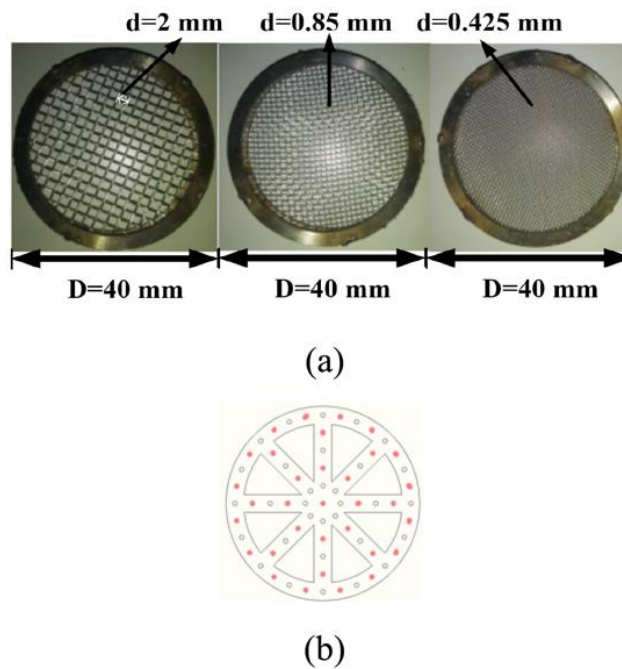

Figure 13: Electrodes Structure and Arrangement.

Chapter 3: Methodology and Simulation

In this chapter we will introduce the new structure design and discuss the possible ways to verify it and validate the resultant ionic wind velocity, additionally; it represents the results of the simulation for proposed design.

As mentioned in Section 2.4.3 in terms of Multi-Needle to Net Electrode structure, the resultant ionic wind velocity of the whole structure is affected by several factors depending on the structure design and revealed that the electric field of a particular needle is affecting the other needles and evaluating the resultant wind velocity in a multi-needle to net electrode structure configurations is not straightforward. Thus, it is more robust to study an established design and evaluate the results either by experimental setup or simulation.

It is applicable to validate a design experimentally by utilizing the technology of the Schlieren System which is shown in Figure 14 [www.holmarc.com], the system overcomes the fact that it is hard to imagine how air flows can be made visible and provide a powerful technique to visualize fluctuations in optical density of a medium or changes in air flow, depending on light travel throughout the inhomogeneous media when the air in motion, but because the system is not available locally, cost of tools and lead time, it was decided to validate the results using a simulation software which is called ANSYS FLUENT.
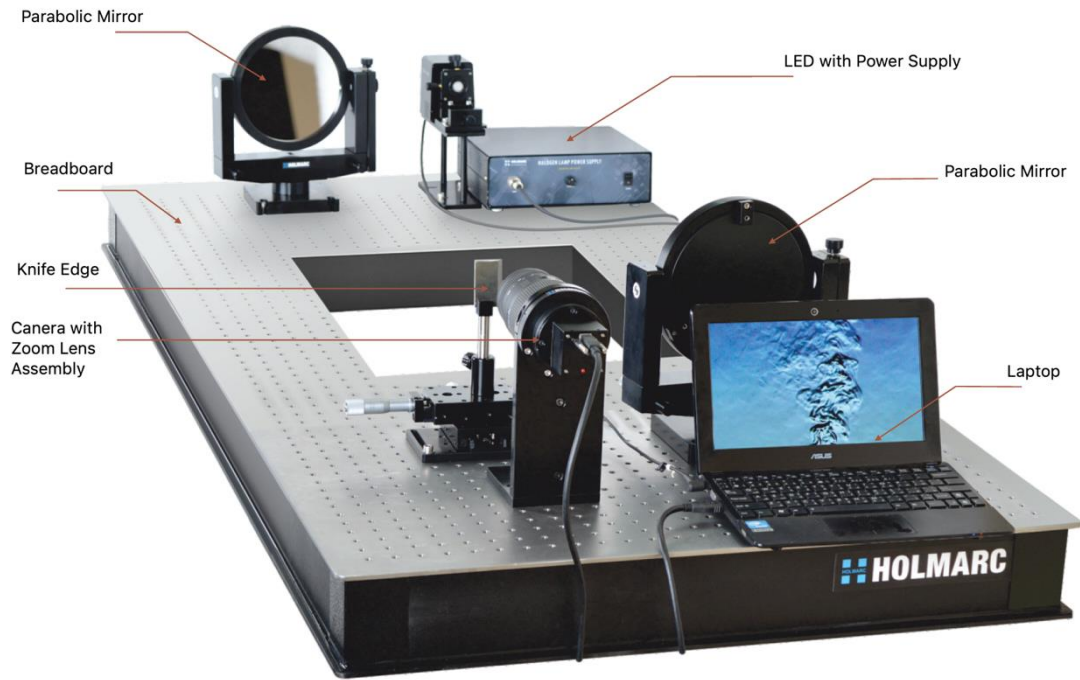
Figure 14: Schlieren System.

3.1 Brief Description of Simulation Software

Ansys Simulation Software is a computer program for modeling heat transfer, fluid flow, and chemical reactions in complex geometry, the software run, and services based on the Finite Element Method (FEM) principle, FEM has become an integral part of the design and development of numerous engineering systems.

Analytical Methods can be used to solve a boundary condition problem but they are applicable only for simple geometry, but for complex geometry, the Numerical Methods are more robust, the FEM is a numerical method that is used to obtain an approximate solution for a given boundary condition problem, for complex geometry similar to the design targeted in this thesis, the software divides the space into smaller pieces (Meshing) where space becomes many small elements and the cross of each line with another is called Node, accordingly, computer shall calculate the values and solve the problem for each element taking into consideration the values of neighbor elements to print the final results, the Figure 15 illustrates the process of FEM which is followed by the Ansys Software.
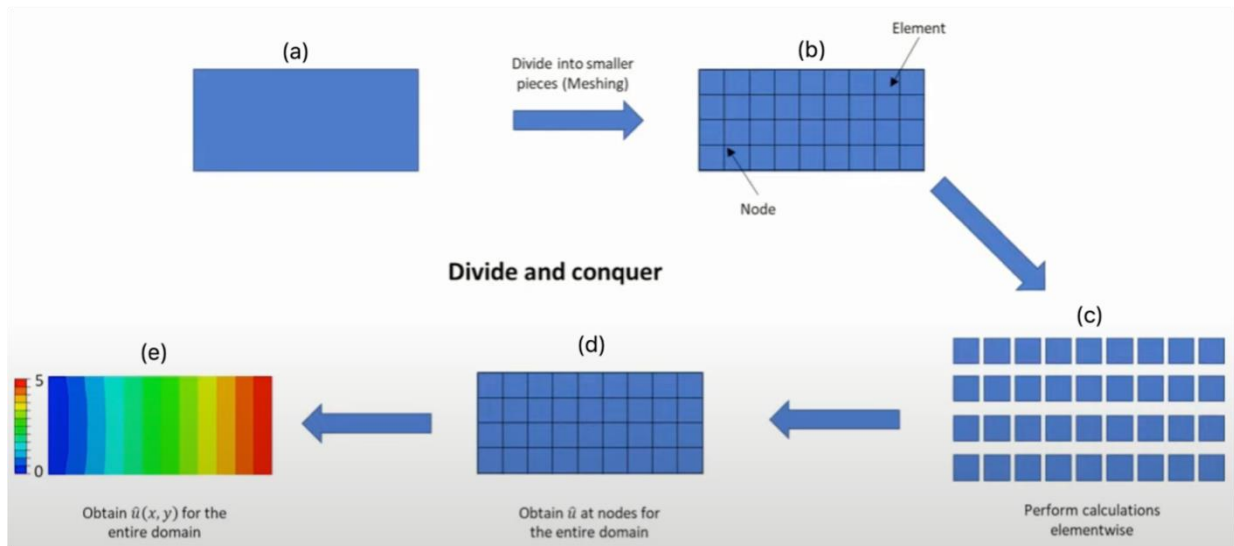
Figure 15: Basic Process of FEM [Ansys Fluent User Guide].

(a) whole space or domain of the problem that need to be studied. (b) meshing the complete domain into small elements, the cross section between each neighbor elements called "node". (c) calculate the results for each element after considering each element as a domain of separate problem. (d) system will obtain the values of results for each node at each element corners to be gathered later. (e) assemble all values together to obtain the results for the entire domain.

3.2 Geometry and Design Parameters

To study the resultant ionic wind velocity and validate the airflow generated by an ionic wind generator, a model of Multi-Needle to Net Electrodes has been designed using the software of Design Modeler and drawn from the scratches to meet the expected results, following figures illustrate the built geometry where 25 needles were designed perpendicular to a Net Electrode, each needle length is 7 mm with a radius of curvature at the needle tip 100 μm, the radius at the bottom of the needle is 1 mm. On the other side, a Net Electrode with a diameter of 50 mm is designed with a side length of 12 mm.

Additionally, containers were built around the design to define the boundary conditions of the system along with cylindrical containers used to densify the mesh around the electrodes which would improve the calculation accuracy (refer to Figure 16), besides that, the design is limited to software capabilities and accordingly, it is expected that if the validation had been implemented experimentally, improved results might be achieved, for example, the needles tip curvature could be less than 100 μm which will

improve the system in terms of breakdown voltage and resulted in an improved ionic wind velocity.
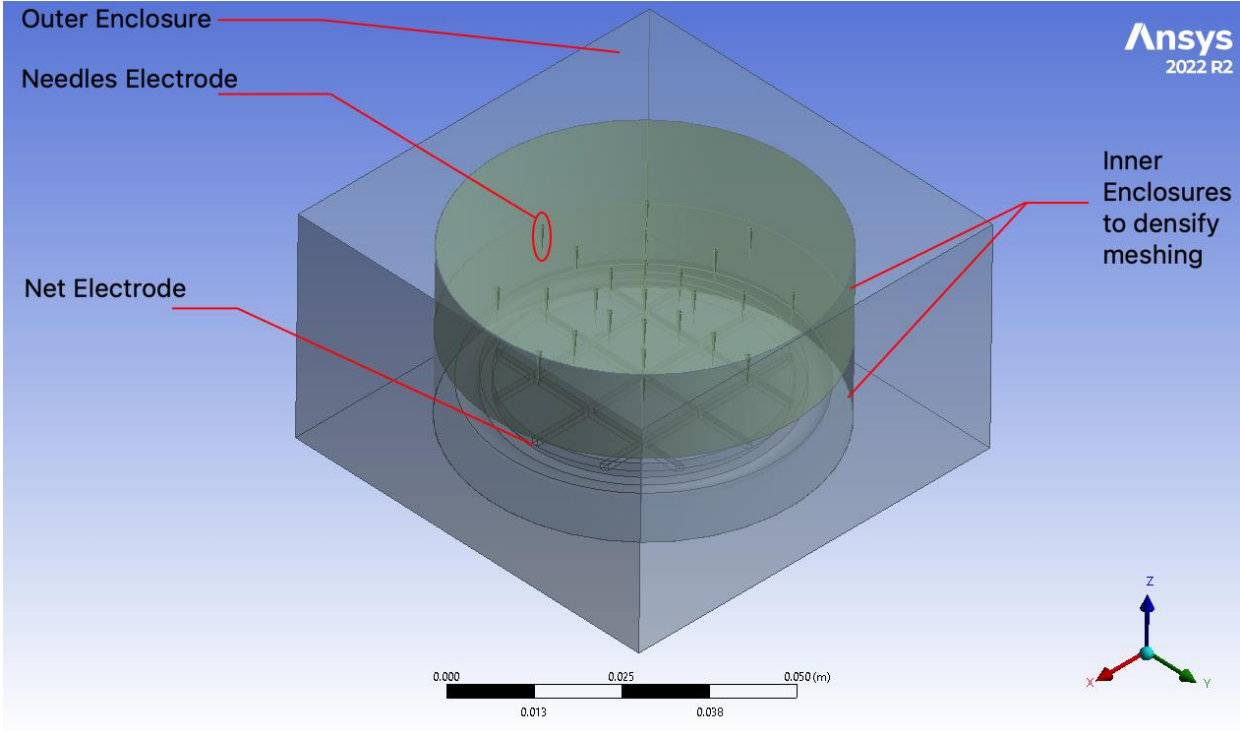

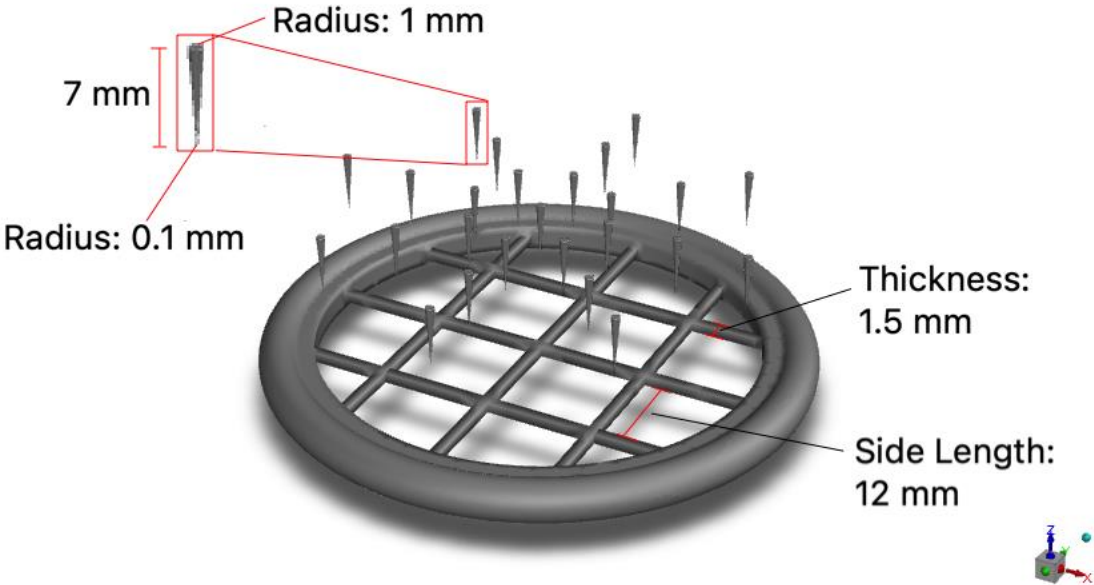Figure 16: Full Geometry of Multi-Needle to Net Electrode.

Figure 17: Geometry without Containers.

About the software sequence of such simulation, the meshing of space between electrodes was performed using the unstructured grid as shown in Figure 17, the meshing of the space is mainly to transfer the system to be a discrete number of elements where the software will be able to measure certain parameters on each element and generate the results, finally, 2,504,901 elements are generated to calculate the ionic wind velocity on each point and calculate the maximum velocity can be achieved by this design, the meshing process has been densified near the electrodes to obtain accurate data as shown in Figure 18.
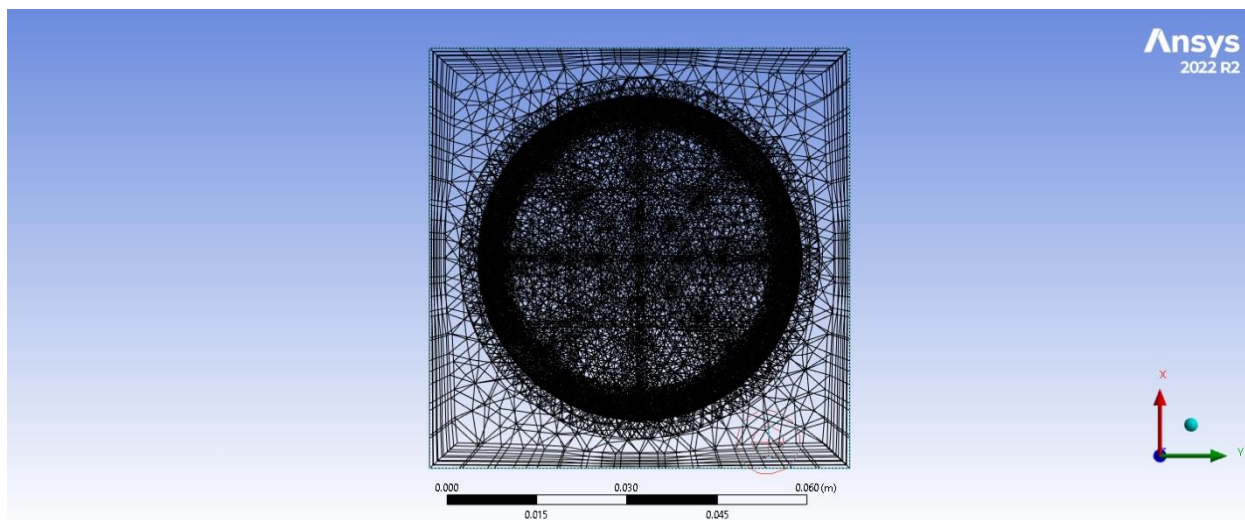

Figure 18: Unstructured Mesh of the Geometry.

After meshing, there are many steps performed to configure the software project to calculate the resultant air velocity, during the setup section, an Electrohydrodynamic Model (EHD) has been activated to assign the positive potential on Needle-Electrodes where the simulation was run for three values separately (10K, 15K, and 20K) volts, and to assign the Zero volt as a negative electrode for Net-Electrodes. Then the material of design was selected as Air for the space around the electrodes, Aluminum for both Needle and Net Electrodes, after that, boundary conditions were configured for the inlet velocity to be Zero m/s so we can obtain the resultant air velocity generated based on the electric field only, and the boundary condition for the electrodes with a voltage mentioned above.

3.3 Simulation Results

Cross-sections was built horizontally near the needle's tip to realize the wind velocity distribution within the whole geometry and another vertical in the middle of geometry as shown in Figure 19, based on the resultant contours, it is clear that the wind velocity is higher in the middle of the circle, and this is expected before the simulation since each needle ionization zoon is affected by the other needles, in general, the air pattern starts from the positive needles electrodes toward the negative net electrode and generating the wind concerning the voltage difference between electrodes.
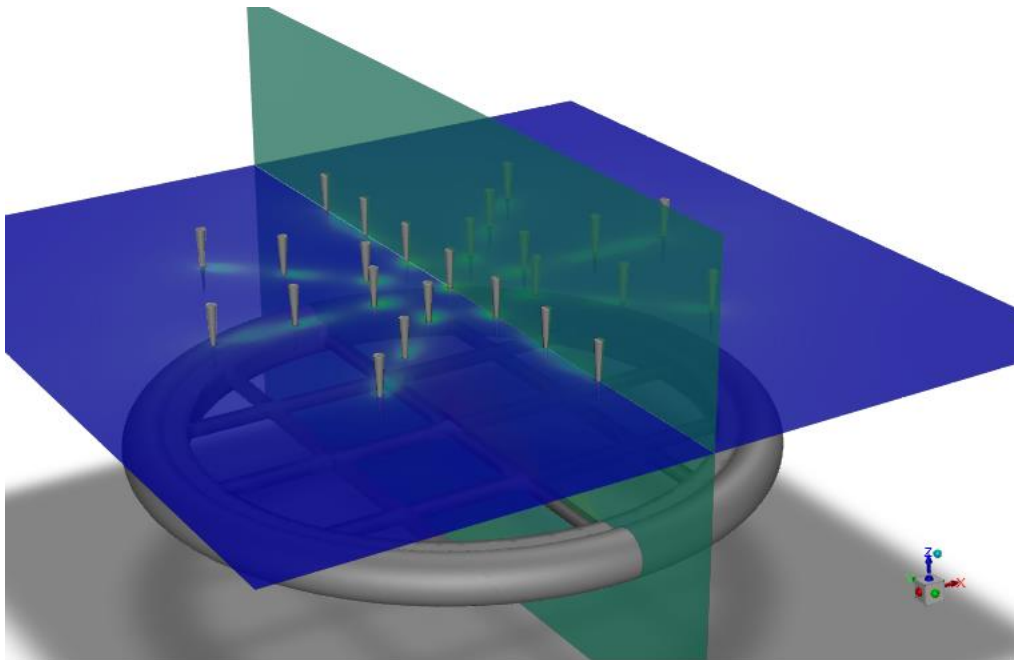

Figure 19: Vertical and Horizontal Cross Sections.

About above said design parameters and established geometry, and after setting up all system registration, in the solution section of Ansys Software, a report of resultant ionic wind velocity is requested. Initially, Needles-Electrode is charged with 10 KV to verify the simulation results, and the simulation is initialized to interpret the results, before printing the results, a cross-section from the middle of the geometry was built

symmetrically to draw the resultant velocity contour as shown in Figure 20 and Figure 21, the maximum ionic wind velocity achieved was 7.16 m/s.
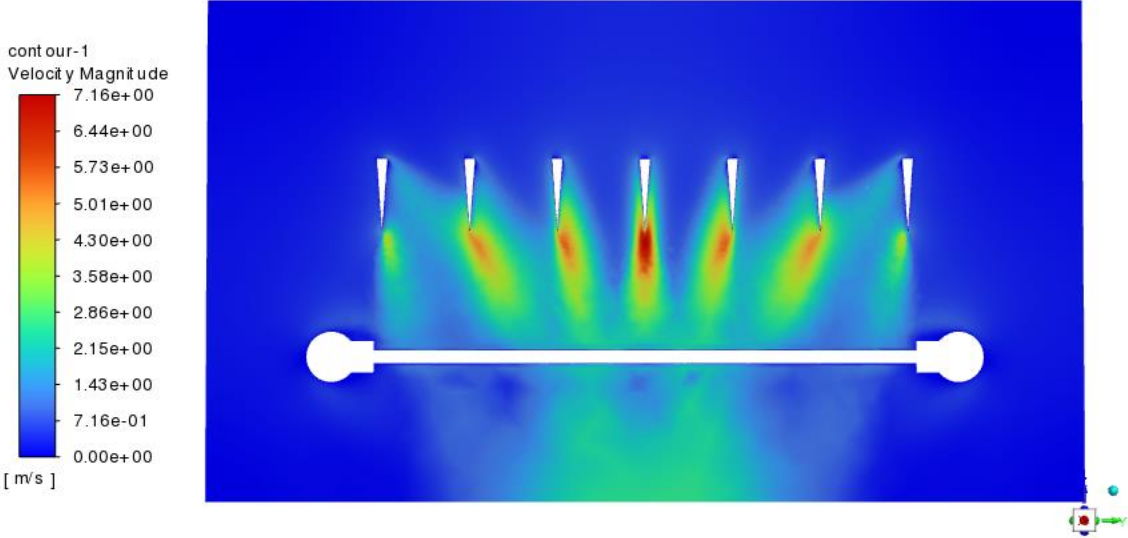

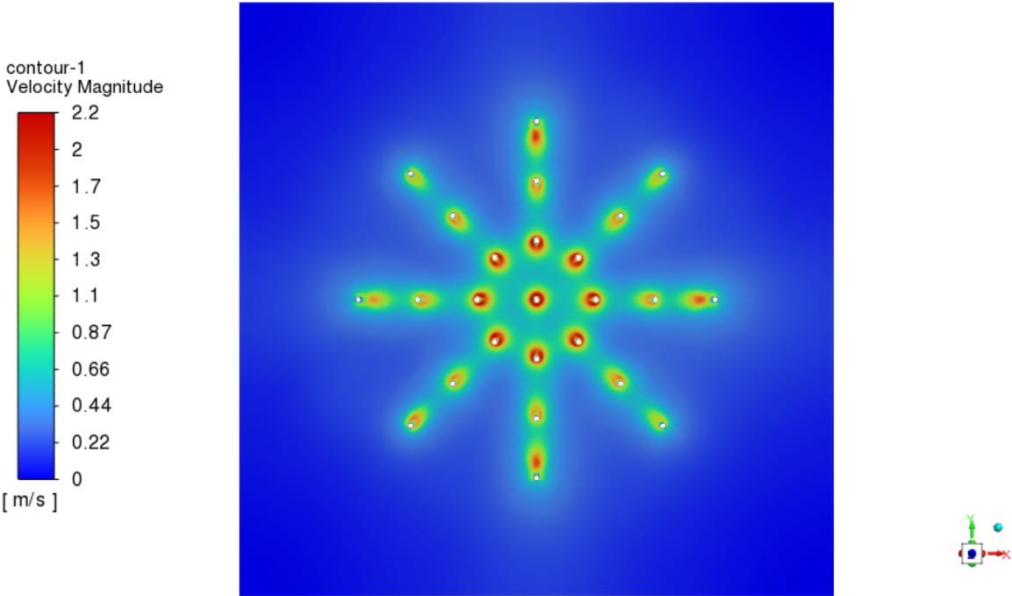Figure 20: Wind Velocity at 10K Volts – Vertical Contour.

Figure 21: Wind Velocity at 10 K Volts, Horizontal Contour.

In addition to the wind velocity, the static pressure distribution was applicable to be shown and generated in Figure 22, numerically, the pressure term is represented in the continuity equation for a steady-state incompressible Newtonian fluid (G. W. Zhang et al., 2021b).

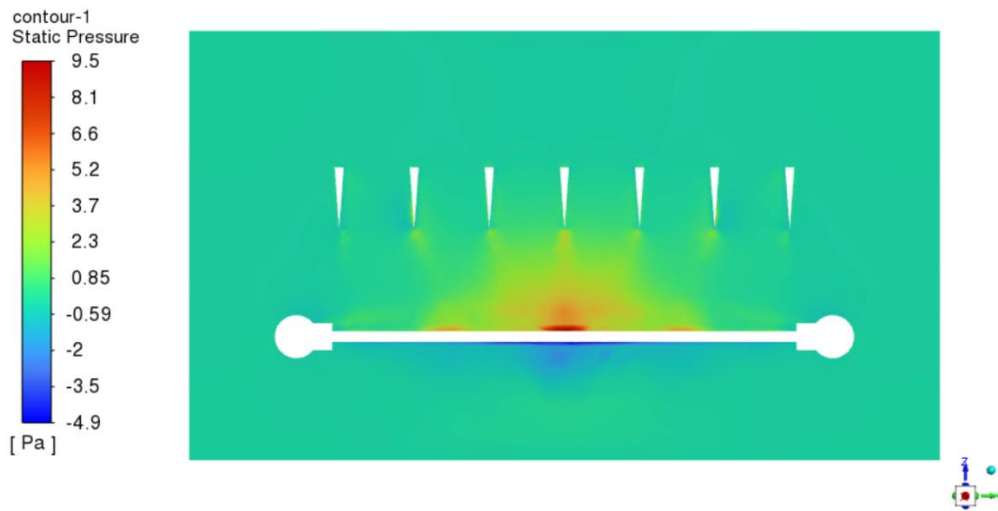$$\nabla.(\rho UU) = -\nabla P + v\nabla^2 U + F \qquad (3.01)$$

Figure 22: Static Pressure Distribution in the Domain at 10 KV.

Similar to the case of 10 kV, the simulation was performed again to verify the resultant outlet velocity influence of applied voltage, and a 15 kV was applied to the Needles Electrode at this time, the resulted ionic wind velocity was significantly higher than the previous attempt, maximum velocity achieved was 8.6 m/s as shown in the Figures 23 and 24.
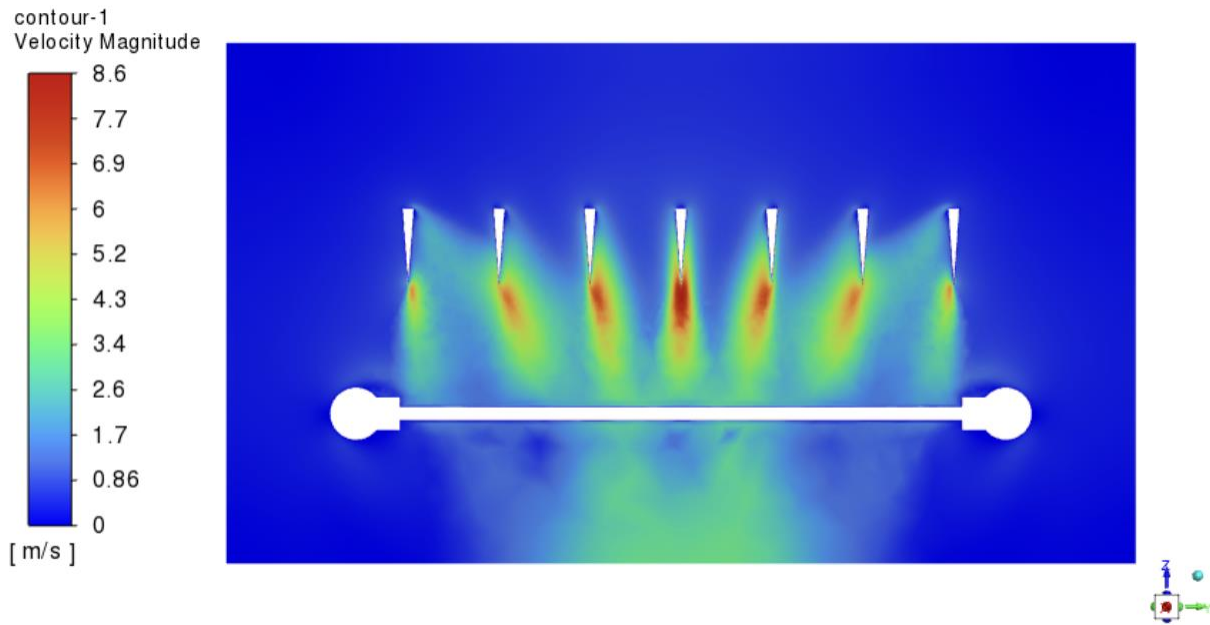
Figure 23: Ionic Wind Velocity at 15 K Volts, Vertical Contour.
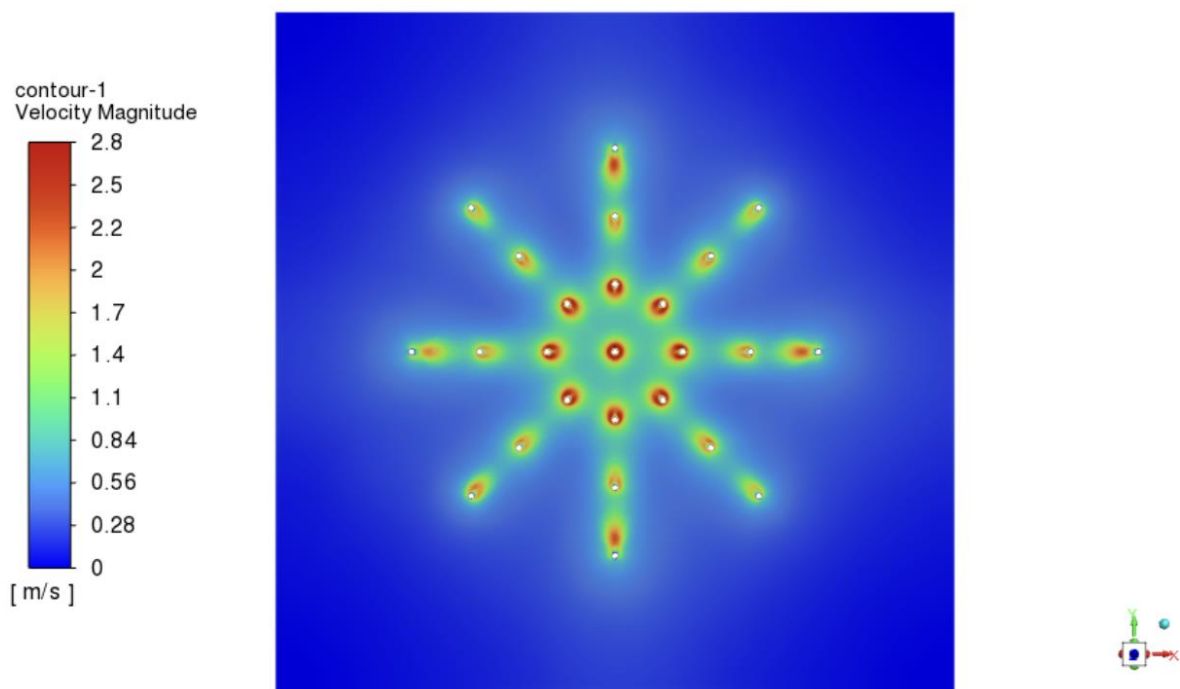

Figure 24: Wind Velocity at 15 K Volts, Horizontal Contour.

At 15 kV, not only the wind velocity was increased, but the static pressure as well, as shown in Figure 25, the pressure at 15 kV has become 15 Pa while it was only 9.5 Pa at 10 kV.
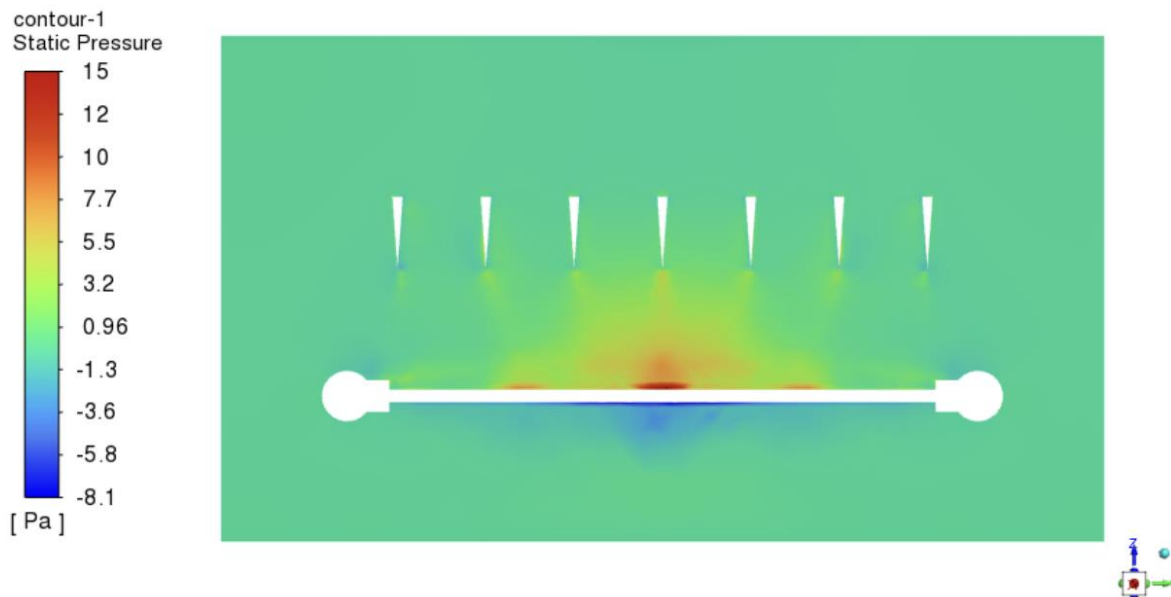
Figure 25: Static Pressure Distribution at 15 KV.

Based on the above data, it was preferred to investigate the resultant wind velocity at higher voltages since the results were enhanced and increased with the increase of voltage, therefore, a 20 kV was applied again on the Needles Electrode and the results are shown in Figure 26 and 27 as a horizontal and vertical contour for wind velocity along with the static pressure contour as shown in Figure 28.
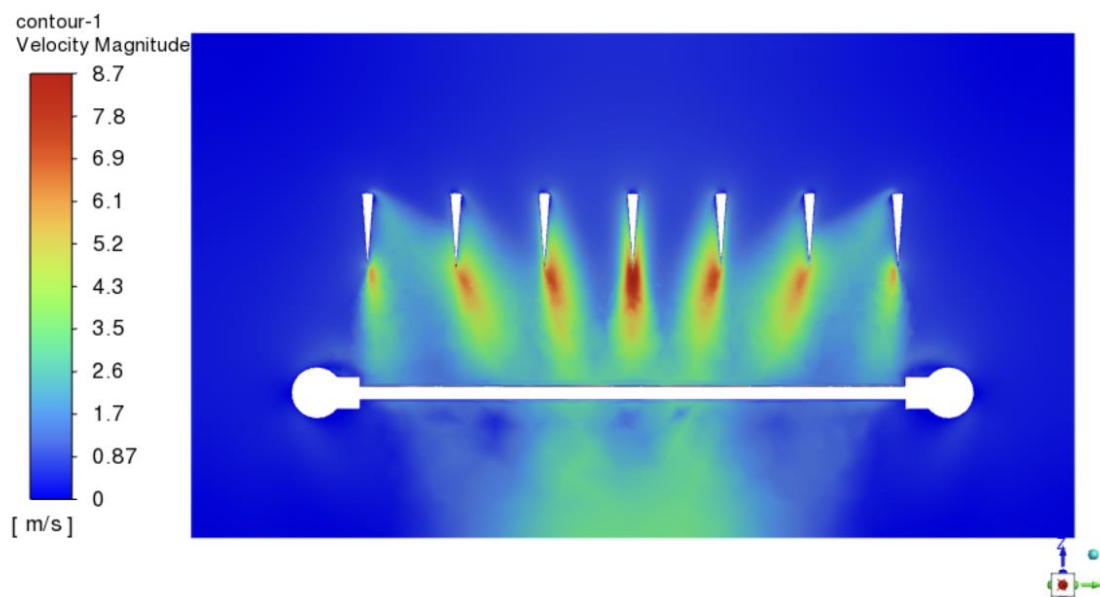

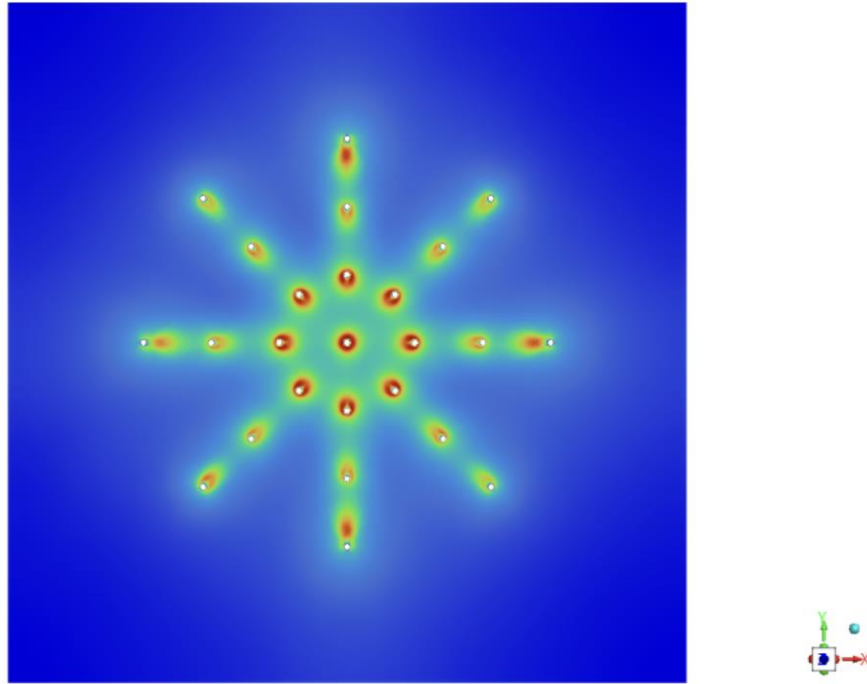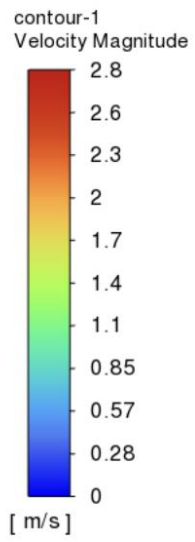Figure 26: Ionic Wind Velocity at 20 K Volts, Vertical Contour.

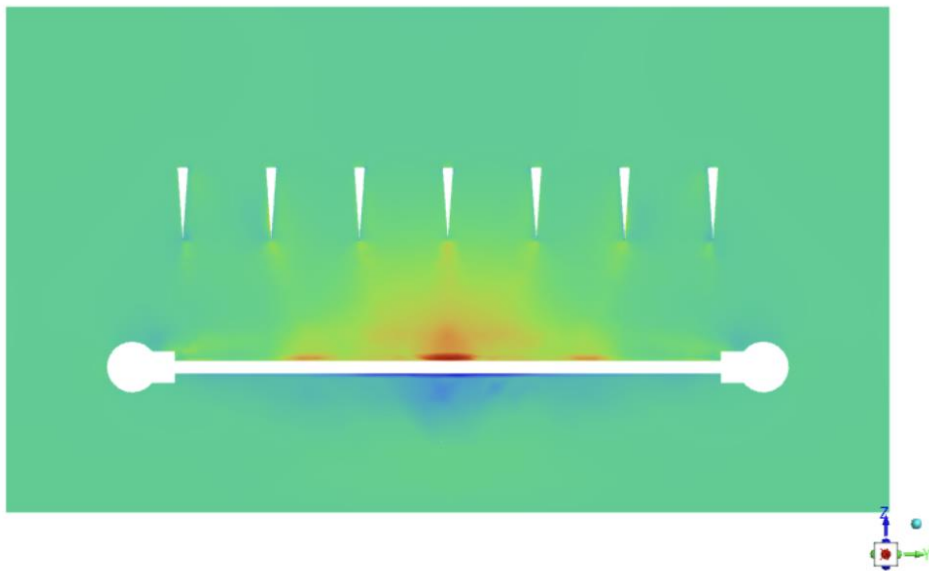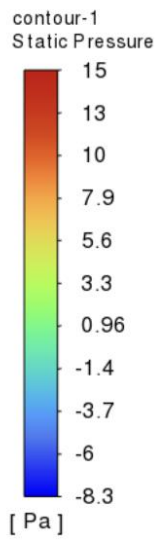Figure 27: Wind Velocity at 20 K Volts, Horizontal Contour.

Figure 28: Static Pressure Distribution at 20 KV.

In addition to above, an image processing has been performed on the figures of horizontal section for the ionic wind velocity for more data visualization and exploration, Figure 29 shows the 3D plot of the velocity and evaluates the magnitude at a grid of points in the X-Y plane, draws a 3D surface showing how the resultant velocity varies across the plane, and it emphasize the magnitude of wind velocity is higher at the tips of the needles and became lower gradually away from the needle location, furthermore, the velocity magnitude between the needles remains feasible since each needle affect and support the neighbor one.

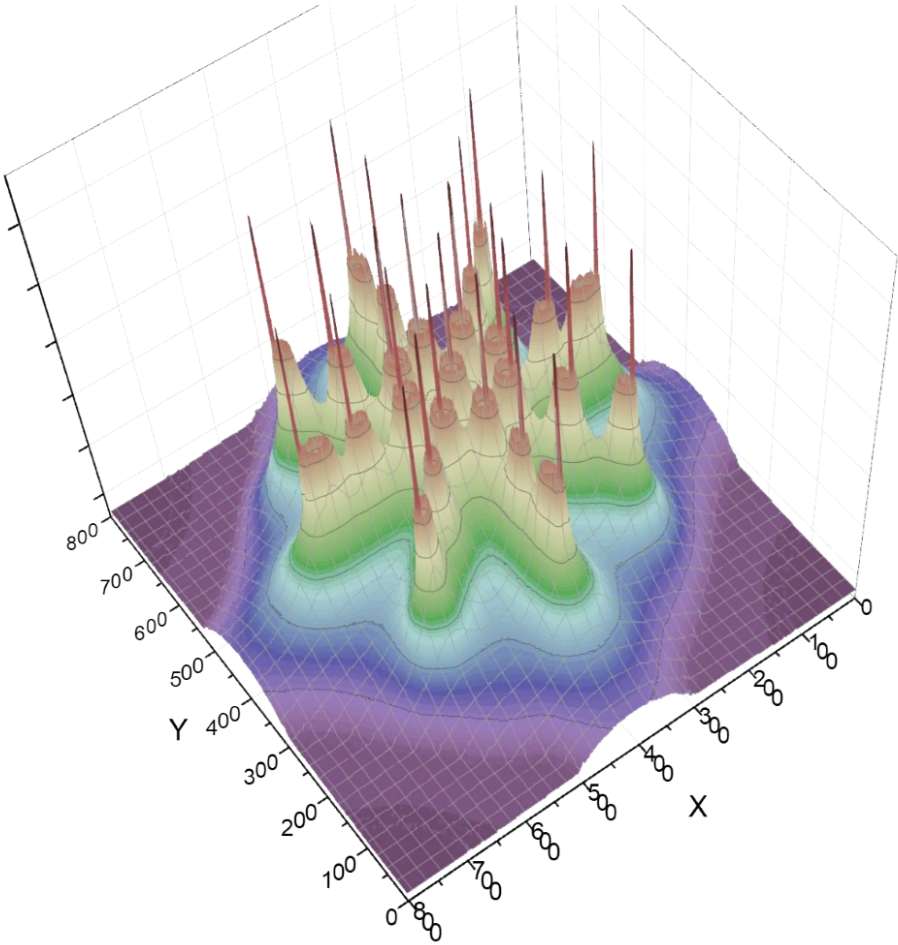Figure 29: 3D Plot of Ionic Wind Velocity Magnitude.

Similarly, to visualize the data resulted from ANSYS Fluent, the resultant static pressure for all three simulations have been analyzed for comparison purposes, and the results shown in Figure 30 show the magnitude of static pressure for each simulation across the diameter of the ionic wind producer, the pressure was high at the center of the

geometry reaching 9.5 Pa during first simulation when we applied 10 KV voltage, on the other side, both 15 KV and 20 KV simulations resulted maximum 15 Pa pressure at the center, therefore, it can be concluded that the resultant ionic wind velocity and pressure increases with the increase of applied voltage but up to a certain limit.
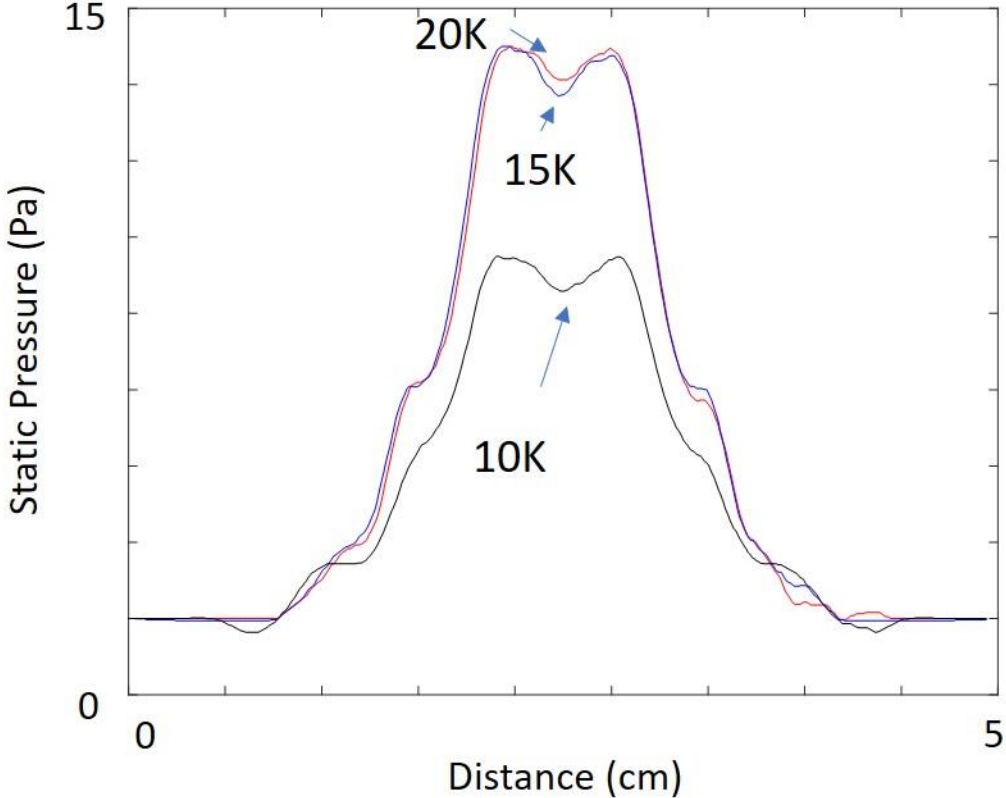
Figure 30: Resultant Static Pressure for all Three Simulations.

Finally, according to the results of the three simulations, it can be realized that with the increase of the electric potential, the velocity speed increase but up to a certain limit, and the relationship is not linear, based on the above, 15 KV generate the optimum resultant velocity with minimum power consumption.

3.4 Application of the Design

About the above case study, design, and simulation, it is worth finding an answer to the question "what is the application of such design that would benefit humans and participate in the race of technology?", to answer this question, we start from the design mentioned in the previous section and start building on it, we consider that above design

of ionic wind producer (which is 5 cm diameter) as a sector of a sphere as illustrated in Figure 31. One sphere will represent an ionic wind generator which is built by connecting several wind producers, in general, the inner sphere would be manufactured by connecting the sectors of negative net electrodes and aligned with the outer sphere which is containing the positive needles electrodes.
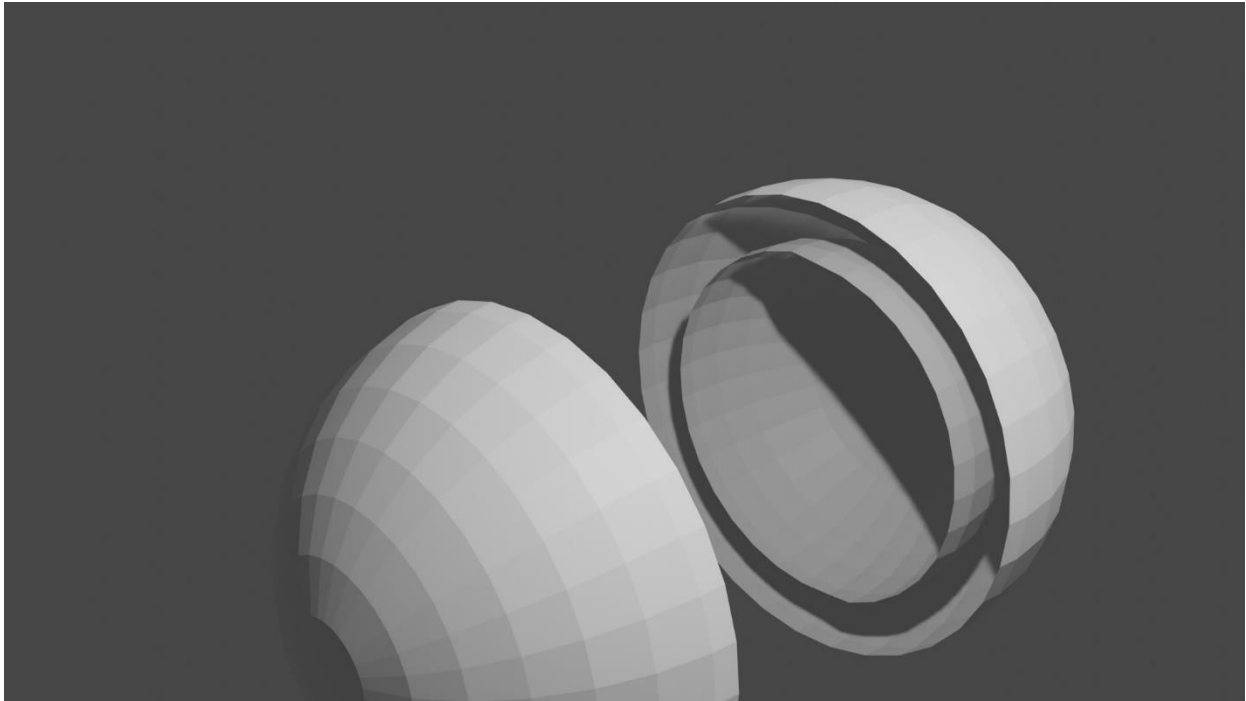
Figure 31: Single Ionic Wind Generator.

The design of the sphere and the location of each sector for each wind producer should take into consideration the airflow because all producers will be connected and powered by an electronic selector since they are not supposed to be activated at once, this concept should allow us to activate and power on the sectors/producers that needed based on required airflow direction, for example, the upper portion of the sphere might be activated to generate airflow downward while the bottom portion is off.

In consistency with the above design for the Ionic Wind Generator, a such device might be arranged and built for an airplane or drone to take off and fly, in addition to that, four generators can be assembled as shown in Figure 32 to produce more airflow,

the advantages of using more than one generator are to increase the thrust force for airplane/drone takeoff and enhance the control of flight balancing and directions.
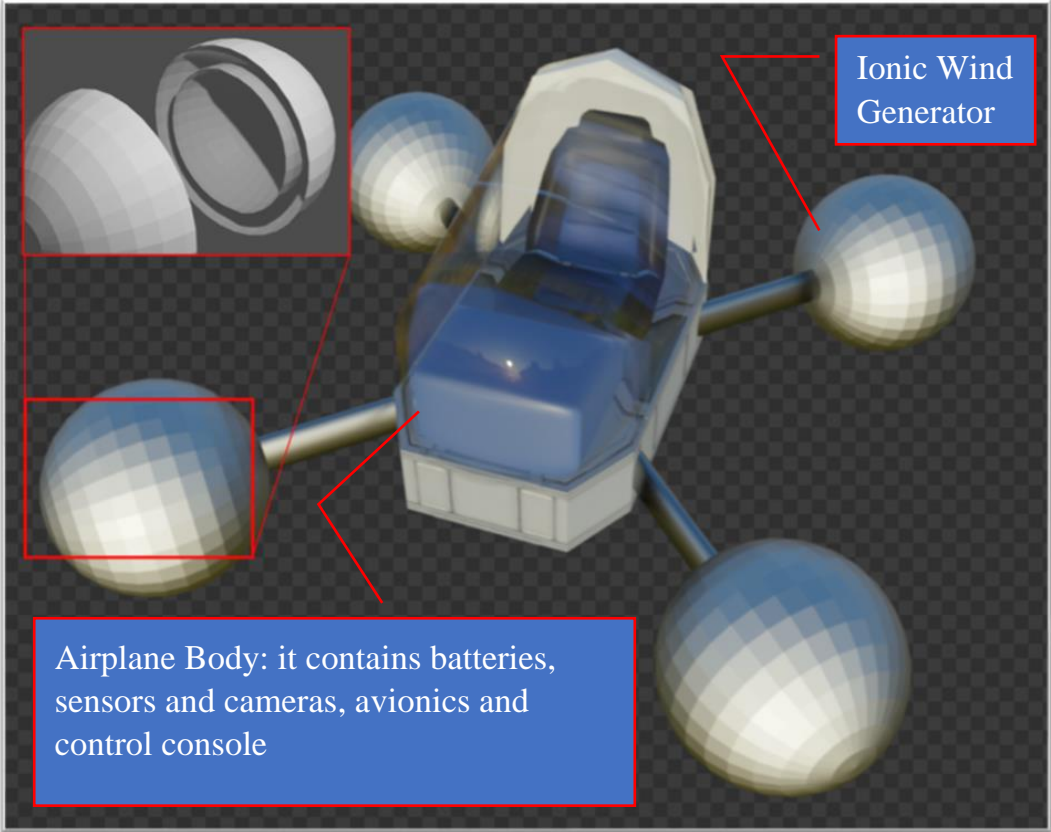
Figure 32: Design of an Airplane with Ionic Wind Generators.

As shown in Figure 32, four generators are assembled with the main body of the airplane, the body would be including the seat of the pilot, a console to control the airplane, batteries to power the airplane, a power converter, sensors, and cameras for data collection, and avionics such as selector to control the needed activated sectors of each generator depending on required thrust, speed, and direction of flight.

Chapter 4: Conclusion

This Chapter concludes the thesis results, clarifies the limitations and challenges faced during the study, and proposes future work.

In this thesis, the nature of ionic wind generation has been validated and verified using simulation software (ANSYS Fluent), it recapped the previous works of literature studied ionic wind generation in terms of resultant wind velocity and verified the best design that generates the maximum wind velocity, and reference to the simulation results, it was clear that the design of Multi-Needle to Net-Electrodes can generate the maximum ionic wind velocity.

Based on this study, it has been concluded that several factors affect the wind velocity such as the geometry design of electrodes, the gap distance between electrodes, and the applied voltage to power the generator, in particular, it was found that increasing the number of needles in the positive electrode will increase the ionic wind velocity, and therefore, after simulation, it has been suggested in Section 3.4 to assemble more than one ionic wind producer/sector in a spherical shape to build a single generator, and then assemble four generators to provide more thrust power to the whole application.

Additionally, it was verified that based on each design, there is an optimum voltage amplitude to provide the best ionic wind velocity with the minimum power efficiency, in our case and design, it was found that 15,000 Volt is robust and enough to produce the maximum velocity that such design can produce as shown in Table 2 and Figure 33, where the velocity almost reaches the saturation line beyond 15 kV, following table summarizes the velocities resulted by each applied voltage amplitude.

A High-Voltage power converter (HVPC) can be used in three stages (2.5X, 15X, and 5.6X) to reach around 15,000 Volts, using 20 cells of Lithium-ion batteries in series, each is 3.7 V and totally will produce 74 Volts, HVPC includes three stages, a series-parallel resonant inverter to convert the DC current to a high-frequency alternative current, then a high voltage transformer and finally full-wave Cockcroft-Walton multiplier shall rectify the high frequency AC back to a DC, at the end, the output of this arrangement will be 15,540 Volt.

Table 2: Results of Simulation based on Applied Voltage.

Applied Voltage (kV)	Ionic Wind Velocity (m/s)	Static Pressure (Pa)
10	7.16	9.5
15	8.6	15
20	8.7	15
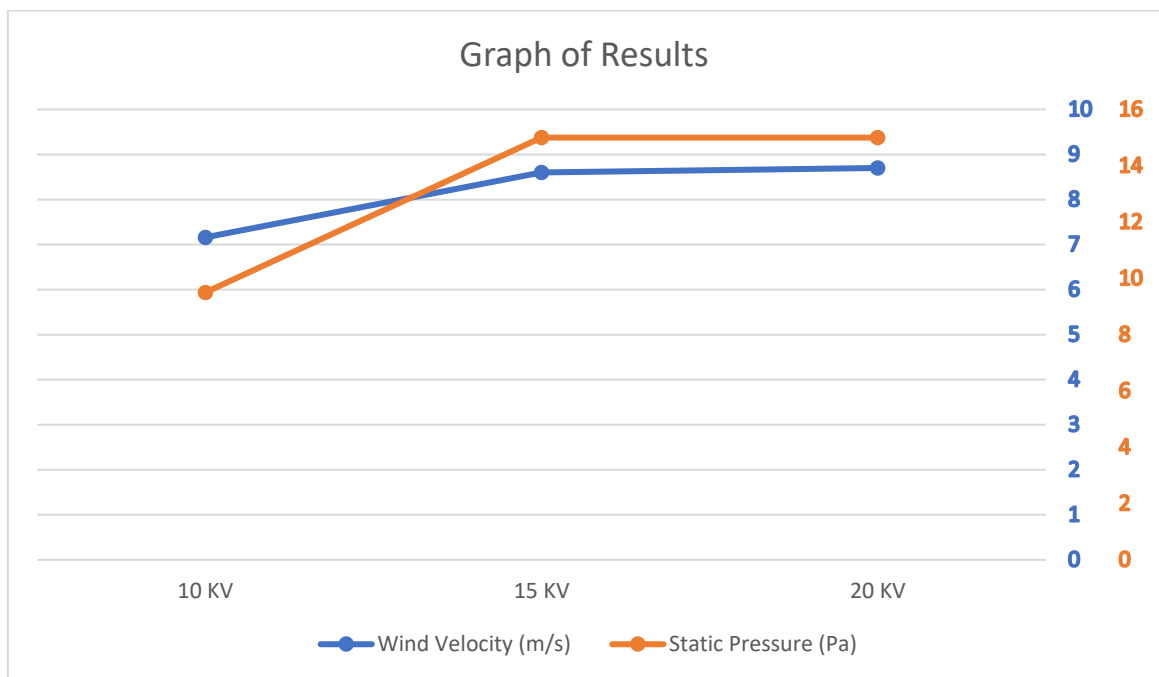
Figure 33: Graph of Simulation Results.

Indeed, it should be noted that there were some limitations faced during this thesis, lack of instruments and tools for the schlieren system to perform experimental results to be compared with simulation results was the biggest limitation, the above-simulated design could be made physically and the results of the ionic wind velocity can be visualized using schlieren system and measured by an accurate speed sensor, in

addition to that, ANSYS software was not available easily and initially, there was a lot of attempts performed using ANSYS student version, which is limited to 500,000 elements during meshing stage, in reality, this number of elements is not enough for our design, therefore we overcome this challenge by renting an HPC (High-Performance Computer) using cloud technology and including a full version of the software.

Finally, this study can be extended in the future by experimental validation using proper tools and instruments, where it can be easier for the researcher to study the case using several designs to verify the resultant velocity under numerous circumstances related to the gap distance, number of needles, distribution of needles and different net electrode side length. In addition to that, the most interesting future study would be performed with the cooperation of aviation engineers to build a prototype of the suggested drone and reach the point of maximum airplane/drone speed that can be achieved using those generators.

References

Adamiak, K., & Atten, P. (2004). Simulation of corona discharge in point-plane configuration. *Journal of Electrostatics*, *61*(2), 85–98. https://doi.org/10.1016/j.elstat.2004.01.021

Chang, J. S., Lawless, P. A., & Yamamoto, T. (1991). Corona Discharge Processes. *IEEE Transactions on Plasma Science*, *19*(6), 1152–1166. https://doi.org/10.1109/27.125038

Chen, J., & Davidson, J. H. (2003). Ozone Production in the Negative DC Corona: The Dependence of Discharge Polarity. *Plasma Chemistry and Plasma Processing*, *23*(3), 501–518. https://doi.org/10.1023/A:1023235032455

Deng, X., & Adamiak, K. (1999). The electric corona discharge in the triode system. *IEEE Transactions on Industry Applications*, *35*(4), 767–773. https://doi.org/10.1109/28.777183

Fylladitakis, E. D., & Kiousis, K. (2008). Ionic wind generation during positive corona discharge in a wire-cylinder air gap Electrohydrodynamic (EHD) Flow in Fluids View project Non linear phenomena in solid dielectrics under the application of high, fast rising electric fields View project. *Certified International Journal of Engineering Science and Innovative Technology (IJESIT)*, *9001*(1). https://www.researchgate.net/publication/280489806

Gilmore, C. K., & Barrett, S. R. H. (2015). Electrohydrodynamic thrust density using positive corona-induced ionic winds for in-Atmosphere propulsion. *Proceedings of the Royal Society A: Mathematical, Physical and Engineering Sciences*, *471*(2175). https://doi.org/10.1098/rspa.2014.0912

Go, D. B., Garimella, S. V., Fisher, T. S., & Mongia, R. K. (2007). Ionic winds for locally enhanced cooling. *Journal of Applied Physics*, *102*(5). https://doi.org/10.1063/1.2776164

J. S. Townsend. (1915). Electricity in Gases. *Nature*, *95*(2388), 611–612. https://doi.org/10.1038/095611a0

Jennifer Chu. (n.d.). *MIT engineers fly first-ever plane with no moving parts | MIT News | Massachusetts Institute of Technology*. Retrieved March 5, 2022, from https://news.mit.edu/2018/first-ionic-wind-plane-no-moving-parts-1121

Lee, J. W., Heo, H., Sohn, D. K., & Ko, H. S. (2022). Analysis and optimization of the electrohydrodynamic (EHD) flow with a wire-to-two-cylinder configuration for convective heat transfer. *International Journal of Heat and Mass Transfer*, *182*. https://doi.org/10.1016/j.ijheatmasstransfer.2021.121959

Lv, F., Song, J., Wang, P., Ruan, H., & Geng, J. (2019a). Influencing factors of flow field of ionic wind induced by corona discharge in a multi-needle-to-net electrode

structure under direct-current voltage. *IEEE Access*, *7*, 123671–123678. https://doi.org/10.1109/ACCESS.2019.2938420

Lv, F., Song, J., Wang, P., Ruan, H., & Geng, J. (2019b). Influencing factors of flow field of ionic wind induced by corona discharge in a multi-needle-to-net electrode structure under direct-current voltage. *IEEE Access*, *7*, 123671–123678. https://doi.org/10.1109/ACCESS.2019.2938420

Masuyama, K., & Barrett, S. R. H. (2013). On the performance of electrohydrodynamic propulsion. *Proceedings of the Royal Society A: Mathematical, Physical and Engineering Sciences*, *469*(2154). https://doi.org/10.1098/rspa.2012.0623

Park, S., Cvelbar, U., Choe, W., & Moon, S. Y. (2018). The creation of electric wind due to the electrohydrodynamic force. *Nature Communications*, *9*(1). https://doi.org/10.1038/s41467-017-02766-9

Peek, F. W. (1920). *Dielectric phenomena in high voltage engineering*. McGraw-Hill Book Company, Incorporated.

Perkins, H. D., & Thompson, W. K. (2009). *An Investigation of Ionic Wind Propulsion*. http://www.sti.nasa.gov

Perkins, J. (2009). Some General Remarks on Corona Discharges. In *Engineering Dielectrics Volume I Corona Measurement and Interpretation*. https://doi.org/10.1520/stp37821s

Rickard, M., & Dunn-Rankin, D. (2007). Numerical simulation of a tubular ion-driven wind generator. *Journal of Electrostatics*, *65*(10–11), 646–654. https://doi.org/10.1016/j.elstat.2007.04.003

Stuetzer, O. M. (1959). Ion drag pressure generation. In *Journal of Applied Physics* (Vol. 30, Issue 7). https://doi.org/10.1063/1.1777003

Tirumala, R., & Go, D. B. (2011). Multi-electrode assisted corona discharge for electrohydrodynamic flow generation in narrow channels. *IEEE Transactions on Dielectrics and Electrical Insulation*, *18*(6), 1854–1863. https://doi.org/10.1109/TDEI.2011.6118623

Warburg, E. (1899). Ueber die Spitzenentladung. In *Annalen der Physik* (Vol. 67, Issue 1). https://doi.org/10.1002/andp.18993030104

Xu, H., He, Y., Strobel, K. L., Gilmore, C. K., Kelley, S. P., Hennick, C. C., Sebastian, T., Woolston, M. R., Perreault, D. J., & Barrett, S. R. H. (2018). Flight of an aeroplane with solid-state propulsion. In *Nature* (Vol. 563, Issue 7732, pp. 532–535). Nature Publishing Group. https://doi.org/10.1038/s41586-018-0707-9

Zhang, G. W., Yang, J. K., & Lin, X. H. (2021a). Numerical simulation on ionic wind in circular channels. *Chinese Physics B*, *30*(1). https://doi.org/10.1088/1674-1056/abb3f4

Zhang, G. W., Yang, J. K., & Lin, X. H. (2021b). Numerical simulation on ionic wind in circular channels. *Chinese Physics B*, *30*(1). https://doi.org/10.1088/1674-1056/abb3f4

Zhang, T., Zhang, Y., Ji, Q., Li, B., & Ouyang, J. (2019). Characteristics and underlying physics of ionic wind in dc corona discharge under different polarities. *Chinese Physics B*, *28*(7). https://doi.org/10.1088/1674-1056/28/7/075202

Zhang, Y., Liu, L., Chen, Y., & Ouyang, J. (2015). Characteristics of ionic wind in needle-to-ring corona discharge. *Journal of Electrostatics*, *74*, 15–20. https://doi.org/10.1016/j.elstat.2014.12.008

UAEU جامعة الإمارات العربية المتحدة
United Arab Emirates University

Ionic Wind concept has become an interesting subject to scientists and researchers around the world due to its impact on several applications such as EHD cooling, EHD flow control, gas pumps, EHD thrust. This thesis contribute in design optimization targeting best ionic wind velocity and investigate the factors influence the outlet velocity to be controlled and applicable for thrust application such as drones and airplanes.

Tha'er Shekh Ibrahem received his Master of Science in Electrical Engineering from the Department of Electrical and Communication Engineering, College of Engineering at UAE University, UAE. He received his BSc in Electrical Engineering from the College of Engineering, An Najah National University, Palestine.

www.uaeu.ac.ae

UAEU عمادة المكتبات
Libraries Deanship

جامعة الإمارات العربية المتحدة
United Arab Emirates University

Digital Library Services Section - قسم الخدمات المكتبية الرقمية